Journal International of Modern Engineering
ISSN: 1930-6628
www.ijme.us

INTERNATIONAL JOURNAL OF MODERN ENGINEERING

Fall/Winter 2025
Volume 26, No1

The Leading Journal of Engineering, Applied Science and Technology

Industrial

Electronics

Biomedical

Civil

Aerospace

Computer

Electrical

Chemical

Mechanical

ENGINEERING

THE LEADING JOURNAL OF ENGINEERING, APPLIED SCIENCE, AND TECHNOLOGY

Print ISSN: 2157-8052
Online ISSN: 1930-6628

www.ijme.us

www.iajc.org

INTERNATIONAL JOURNAL OF MODERN ENGINEERING

ABOUT IJME:

- IJME was established in 2000 and is the first and official flagship journal of the International Association of Journal and Conferences (IAJC).
- IJME is a high-quality, independent journal steered by a distinguished board of directors and supported by an international review board representing many well-known universities, colleges and corporations in the U.S. and abroad.
- IJME has an impact factor of **3.00**, placing it among the top 100 engineering journals worldwide, and is the #1 visited engineering journal website (according to the National Science Digital Library).

OTHER IAJC JOURNALS:

- The International Journal of Engineering Research and Innovation (IJERI)
  For more information visit www.ijeri.org
- The Technology Interface International Journal (TIIJ).
  For more information visit www.tiij.org

IJME SUBMISSIONS:

- Manuscripts should be sent electronically to the manuscript editor, Dr. Philip Weinsier, at philipw@bgsu.edu.

  For submission guidelines visit
  www.ijme.us/submissions

TO JOIN THE REVIEW BOARD:

- Contact the chair of the International Review Board, Dr. Philip Weinsier, at philipw@bgsu.edu.

  For more information visit
  www.ijme.us/ijme_editorial.htm

INDEXING ORGANIZATIONS:

- IJME is currently indexed by 22 agencies. For a complete listing, please visit us at www.ijme.us.

Contact us:

Mark Rajai, Ph.D.

Editor-in-Chief
California State University-Northridge
College of Engineering and Computer Science
Room: JD 4510
Northridge, CA 91330
Office: (818) 677-5003
Email: mrajai@csun.edu

www.tiij.org

www.ijeri.org

INTERNATIONAL JOURNAL OF MODERN ENGINEERING

The INTERNATIONAL JOURNAL OF MODERN ENGINEERING (IJME) is an independent, not-for-profit publication, which aims to provide the engineering community with a resource and forum for scholarly expression and reflection.

IJME is published twice annually (fall and spring issues) and includes peer-reviewed research articles, editorials, and commentary that contribute to our understanding of the issues, problems, and research associated with engineering and related fields. The journal encourages the submission of manuscripts from private, public, and academic sectors. The views expressed are those of the authors and do not necessarily reflect the opinions of the IJME editors.

EDITORIAL OFFICE:

Philip D. Weinsier, Ed.D.
Manuscript Editor
Office: 419.372.0628
Email: philipw@bgsu.edu
Department of Applied Sciences
Bowling Green State University-Firelands
One University Dr.
Huron, OH 44839

THE INTERNATIONAL JOURNAL OF MODERN ENGINEERING EDITORS

Table of Contents

Editor's Note: Thermoelectric Generators 3
Philip Weinsier, IJME Manuscript Editor

Power Generation and Efficiency for a Flexible Thermoelectric Structure 5
John Mativo, University of Georgia;
Paul Asunda, Purdue University

Utilizing Machine Learning Multi-Output Regression Methods to Predict Turning Movements at Intersections 12
Somayeh Nazari Enjedani, Boise State University;
Mandar Khanal, Boise State University

Augmented Reality in Foot Palpation: Enhancing Accuracy and Training Medial Cuneiform Bone Localization 26
Michael U. Dakeev, Sam Houston State University;
Suleiman Obeidat, Sam Houston State University;
Fatih Demiroz, Sam Houston State University;
Vicente Lombardo, Sam Houston State University

Instructions for Authors: Manuscript Submission Guidelines and Requirements 31

In This Issue (p.5)
Thermoelectric Generators

Philip Weinsier, IJME Manuscript Editor

At its core, a thermoelectric generator (TEG) is a device that converts heat energy into electrical energy. This is accomplished when there is a temperature difference between two different conductors. Common thermoelectric materials include bismuth telluride (BiTe) for low temperatures, lead telluride (PbTe) for medium temperatures, and skutterudites (a cobalt arsenide mineral containing variable amounts of nickel and iron substituting for cobalt—$CoAs_3$) for high temperatures. TEGs, using waste heat, are generally used for power generation, cooling electronic devices, and powering remote devices with radioisotopes or solar heat. And while TEGs currently face challenges such as low efficiency and high cost, on-going and future research is likely to find new materials and develop advanced systems to improve performance. Thermoelectric materials that show the Seebeck effect are capable of generating an electric voltage in the presence of a temperature difference and are classified into two types: n-type and p-type. N-type materials have extra electrons, while p-type materials lack electrons that, when connected in series with metal electrodes, form a thermocouple, which is the basic unit of a thermoelectric generator.

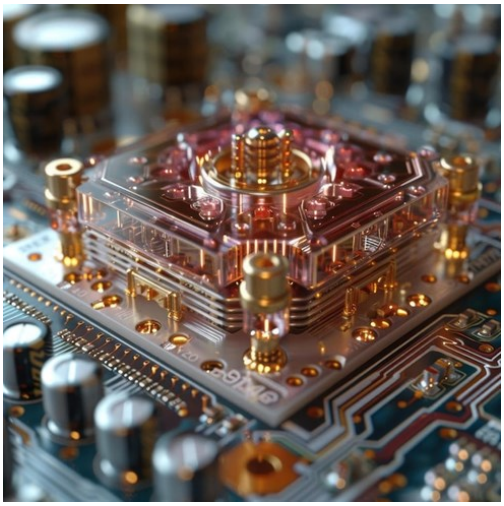

Nanoscale thermoelectric generator on a chip.

A thermoelectric module, then, is made up of many such thermocouples connected electrically in series and thermally in parallel. A thermoelectric module has two sides—a hot side, to be exposed to the heat source, and a cold side, to be exposed to a heat sink. The temperature difference created across the two sides of the module causes current to flow in the circuit. And, as with most any other power source, this resulting current can be used to power an external load or charge a battery. Higher voltages and power outputs depend on the number of thermocouples, the temperature difference, the Seebeck coefficient, and the electrical and thermal resistances of the materials, while the efficiency of TEG is a function of the ratio of electrical power output to heat input. This efficiency is limited by the Carnot efficiency, or the maximum possible efficiency for any heat engine between two temperatures. The actual efficiency of a TEG, however, is much lower than the Carnot efficiency due to various losses including Joule heating, thermal conduction, and thermal radiation.

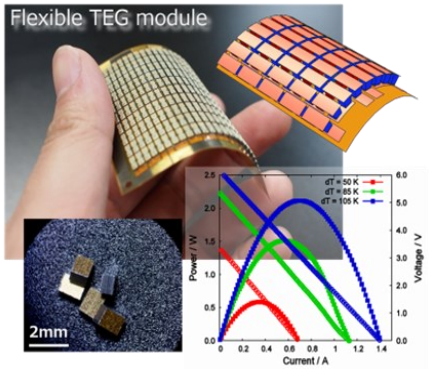

In 1821, Thomas Johann Seebeck (A German physicist) published his novel idea: the generation of an electric current using the thermodynamic properties of the involved materials. This marked a new way to understand thermoelectric phenomena and their implications and paved the way for other researchers to develop other similar ideas. This Seebeck effect would become the basis for thermocouples, TEGs, and other related technologies.

On an interesting historical note, it was William Thomson (Lord Kelvin) who began the study of irreversible processes out of equilibrium by formally analyzing the phenomenon of thermoelectricity.

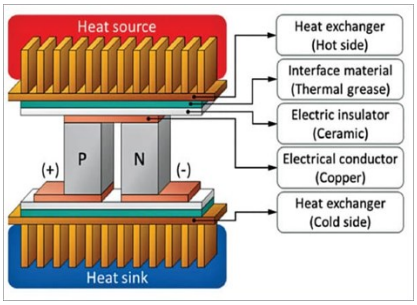

In the featured article in this issue of IJME (p.5), the authors note that while TEGs are robustly built for energy harvesting on planar surfaces and in non-vibratory environments, many waste-heat producing environments are located in non-planar and vibratory areas. Such vibratory areas introduce a challenge for the use of bismuth telluride, as it is a brittle material typically used to make the TEG elements (legs). The authors then respond to the dilemma of how to use TEG devices in non-planar and vibratory environments without experiencing premature structural failures by developing a newly reconfigured composite TEG leg that could provide opportunities to harvest energy in these vibratory environments. The tradeoff would amount to a slightly reduced overall power generation (6%) compared to no access to the free waste energy in these environments.

Editorial Review Board Members

Power Generation and Efficiency for a Flexible Thermoelectric Structure

John Mativo, University of Georgia; Paul Asunda, Purdue University

Abstract

Thermoelectric generators (TEG) are robustly built for energy harvesting in planar surfaces and non-vibratory environments. However, many waste-heat producing environments are located in non-planar and vibratory areas. The non-planar and vibratory areas challenge the use of bismuth telluride, a brittle material that is typically used to make the TEG elements (legs). A dilemma exists of how to use the TEG devices in non-planar and vibratory environments without experiencing a structural premature failure. A reconfiguration of the TEG's legs to incorporate an element of flexibility was used to determine its effects on power and efficiency. Incorporating flexibility in the leg required the removal of some base material from each leg and then either leave it void or fill it with a polymer. In this study, the authors explored three variant configurations of a pair of TEG legs. Findings indicated a viability of reconfigured TEG legs for use in vibratory environments at the cost of reduction in power generation and efficiency.

Introduction

Thermoelectric generators (TEG) are designed to convert waste heat into electricity. Waste heat is a byproduct of a process that has expended energy. Prime examples of where waste heat can be found include the transportation industry, manufacturing, power plants, buildings, and animals. When harvested, waste heat can significantly improve the efficiency of the process. The challenge with TEGs used in conversion of waste heat into electricity for temperatures up to 230°C is that they are made of bismuth telluride (Bi_2Te_3), a brittle material that breaks easily in vibratory environments. The TEG potential for the future is large. TEG devices are light, reliable, have no moving parts, and can be used in hostile and inaccessible environments (Baskaran & Rajasekar 2025; He, Schierning & Nielsch, 2018; Telkes, 1947). The study of TEG power and efficiency is based on flexible configurations (Mativo, Hallinan, George, Reich & Steininger, 2021). In that study, the authors defined a unit cell as two legs sandwiched between top and bottom covers, as illustrated in Figure 1.

The authors of this current study largely explored how to optimize a thermoelectric generator for a vibratory environment. Most of the work presented here deals with mechanical loading on the TEG structure and how it could be modified to better serve vibratory environments. To better understand the effects of TEG structural modification on power generation, the authors compared a baseline model with a reconfigured model. LeBlanc observed three considerations required for a TEG design: geometry, fill factor, and leg size (LeBlanc, 2014). All three play a large role in the tradeoffs of thermal conductivity and electrical resistivity. The unit cell model was based on the Marlow TG12-6 TEG (Marlow Industries, 2015). The S_1 is a positive leg (p-type) that has fewer electrons than the S_2 negative leg (n-type). The two legs are made of bismuth telluride and one is doped to remove or add electrons.

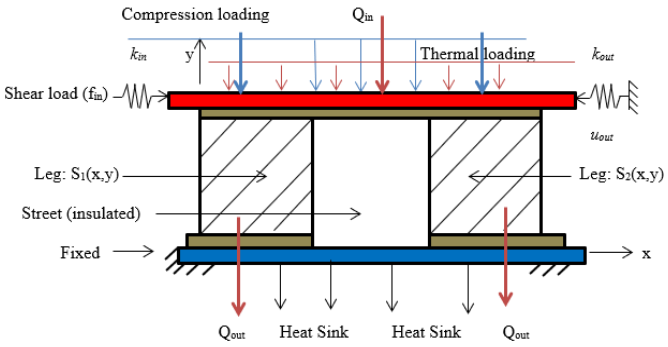

Figure 1. A general unit cell for a TEG subjected to mechanical and thermal loadings (Mativo et al., 2021).

Figure 1 shows that compressive and shear mechanical loading were applied while the bottom surface was considered fixed. This study explored TEG structural flexibility. Further, a uniform thermal load (heat flux) was applied while the bottom, a heat sink, was assumed to have zero thermal resistance. The unit cell legs (S_1 and S_2) were the domains, where the Bi_2Te_3 was placed to support both structural and thermal loads. Figure 2 shows the two domains, where a reduction of Bi_2Te_3 was applied and left void or filled with a polymer. The street between the legs was considered perfectly insulated (Mativo et al., 2021).

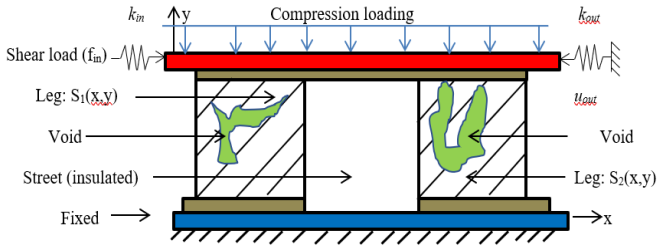

Figure 2. Exploring new structure (Mativo et al., 2021).

Method

In a study by Mativo et al. (2021), the authors discussed in detail the flexibility of a TEG leg structure. In another study by Mativo (2020), the author provided details of the

three TEG configurations and their respective behavior, when structural and thermal loading were applied. The tool used to layout the design domain and create and study the TEG unit cell was a finite element-based tool developed within MATLAB (Mativo, 2020). The intent in this current study was to determine the current produced and the accompanying efficiency of the TEGs. After a general discussion of power generation in TEGs, the authors present three additional parts: a) replication of a previous study to verify the MATLAB tool used to conduct the rest of the experiments; b) application of the verified tool to a Marlow TG12-6 used as the baseline of the experiments; and, c) a unit cell with legs that have a polymer filling the void spaces.

Power Generation

Power generation within a TEG is controlled by the Seebeck, Joule, and Thomson effects. The Seebeck effect describes how temperature difference between two dissimilar conductors produces electromotive force (emf) between them. For this case, the p-type leg contained a positive charge, while the n-type leg held a negative charge. The emf was a catalyst for the thermally excited electrons to move, resulting in current flow. To better illustrate the differences in the legs, ALGOR was used to visually display the results in color. Figure 3 shows how a heat source of 230°C was applied on the left side and a heat sink of 50°C was applied on the right. The figure further shows that, although the temperature distribution along the legs was the same, a maximum heat flux value of 349,894 J/m^{2}s was generated on the left n-type leg of Figure 4, while a minimum heat flux value of 1679 J/m^{2}s was found on the right side on the p-type leg. This action is represented in Equation 1:

$$\alpha = V / \Delta T \tag{1}$$

where, α is the Seebeck coefficient, V is electromotive force or voltage, and ΔT is difference between hot and cold temperatures.

Figure 3. Temperature distribution in a unit cell.

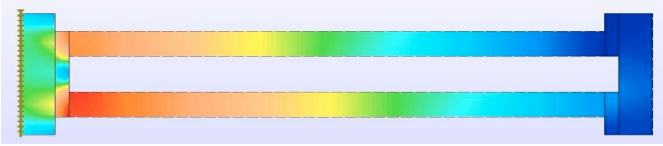

Figure 4. Heat flux distribution in a unit cell.

Joule heating happens when current flows through a material that offers resistance to flow. The amount of heat produced is represented in Equation 2:

$$Q_j = I^2 R \tag{2}$$

where, Q_j is joule heating, I is current, and R is electrical resistance.

The Thompson effect relates to the rate of generation of heat resulting from the flow of current along an individual conductor with a temperature difference (Olivares-Robles, Badillo-Ruiz & Ruiz-Ortega, 2020; Ruiz-Ortega, Olivares-Robles & Ruiz, 2018; Saqr & Musa, 2009; Rowe, 2006). The Thomson effect is represented in Equation 3:

$$Q_t = \beta I \Delta T \tag{3}$$

where, β is the Thomson coefficient, Q_t is the rate of reversible heat absorption, I is the current flow, and ΔT is temperature difference between the ends of the conductor.

The performance of the TEG is greatly influenced by the figure of merit (Z), as shown in Equation 4:

$$Z = \frac{\alpha^2 \sigma}{k} \tag{4}$$

where, $\alpha^2\sigma$ is the electrical power factor and k is the thermal conductivity.

Multiplying with temperature, Z becomes unitless and is represented by ZT, a dimensionless figure of merit. A higher ZT is associated with a higher TEG power generation. In order to obtain a maximum figure of merit, the geometry and material properties for the TEG should satisfy Equation 5 (Chen, Meng & Sun, 2012; Kanimba & Tian, 2016; Rowe, 2006; Yang et al., 2021):

$$\frac{A_P^2}{A_n^2}\frac{L_n^2}{L_P^2} = \frac{k_n}{k_p}\frac{\rho_p}{\rho_n} \tag{5}$$

where, A_p is the cross sectional area of the positive leg; A_n is the cross sectional area of the negative leg; L_n and L_p are leg lengths for the negative and positive legs, respectively; k_n and k_p, are the thermal conductivity for the negative and positive legs, respectively; and, ρ_n and ρ_p are electrical resistivity for the negative and positive legs, respectively.

Equation 6 is used to determine power:

$$P = Q_h - Q_c = N\left(\alpha I \Delta T - I^2 R\right) \tag{6}$$

where, P is power, Q_h is the heat source, Q_c is the heat sink, and N is the number of legs.

The equation used to calculate the thermal power efficiency of a TEG is shown in Equation 7:

$$\eta = \frac{P}{Q_h} \tag{7}$$

where, η is efficiency.

These equations and the Marlow TG12-6 leg geometry, where the Bi_2Te_3 material completely fills the TEG legs (S_1 and S_2 domains), were used to create a MATLAB code (tool) to study the power generation and efficiency of various configurations, as noted earlier in this section.

Prior Study and Tool Verification

In their study of power generation and efficiency of uniform, cross-sectional areas of TEG legs, Kanimba and Tian (2016) observed that power as a function of current behaved in a parabolic manner having an optimal power at a specific current, as shown in Figure 5. A higher temperature input resulted in a higher power. The line graphs represent 100°C increments from 200°C to 400°C from the bottom graph to the top, respectively. The temperature on the heat sink was maintained at 100°C.

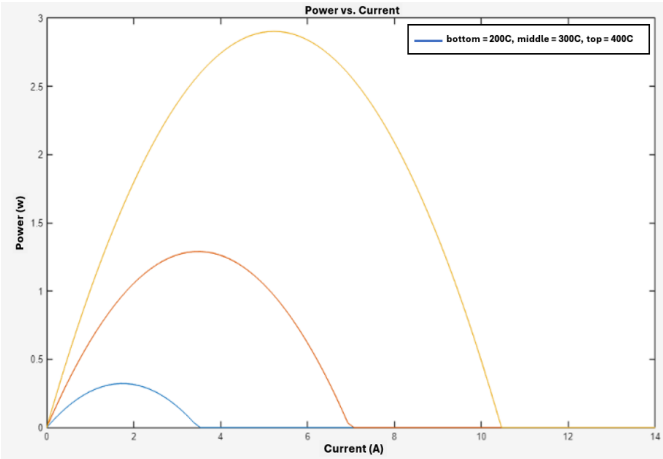

Figure 5. TEG output power as a function of electrical current.

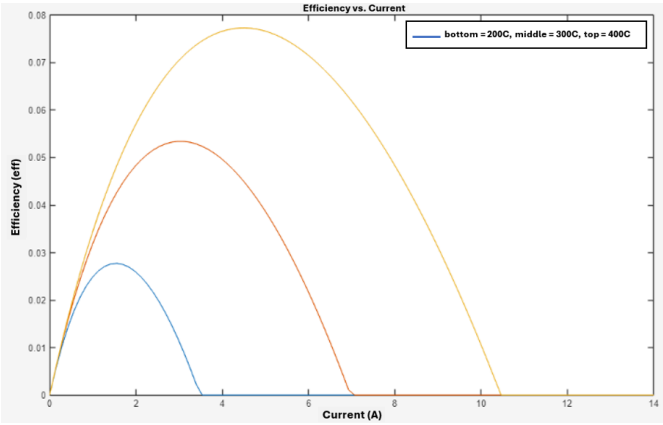

Figure 6. Efficiency as a function of current.

Figure 6 shows efficiency as a function of current for a uniformed TEG leg cross-sectional area. The behavior patterns of the efficiency curve were similar to the power curves. The tool was then used to study the baseline unit cell and the reconfigured composite models.

Baseline Model

The MATLAB tool was used to establish a baseline for comparison of a TEG leg—with a uniform, cross-sectional area—with that of a variable, cross-sectional area. New temperature conditions for this study were used with a high starting from 110°C and rising to 230°C with increments of 60°C. These temperatures correspond to those of the Marlow TG12-6, which was the TEG baseline model for this study. The sink temperature for this experiment was set at 50°C. The parabolic graph of Figure 7 shows the results of the investigation of power as a function of current. The graph also indicates lower values than previously described in the Kanimba and Tian study (2016). The difference was attributed to lower temperatures used.

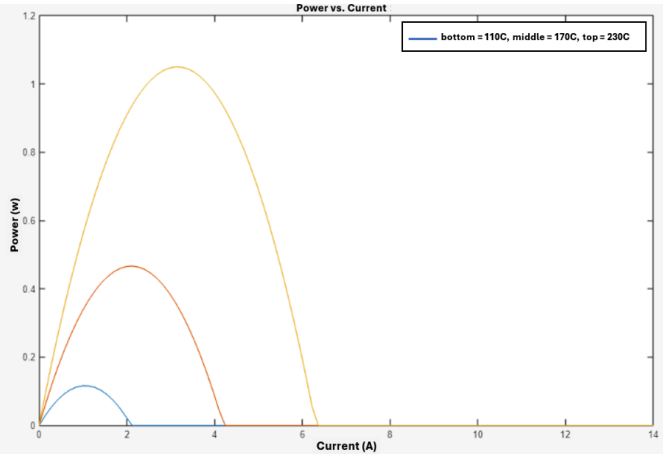

Figure 7. Output power as a function of electrical current for baseline TEG.

Investigating efficiency as a function of current also resulted in the parabolic graph of Figure 8. This graph is similar to the Kanimba and Tian study (2016). Overall, these experiments ran at 36% of those found by Kanimba and Tian. This was expected because of the difference in the temperatures in both experiments.

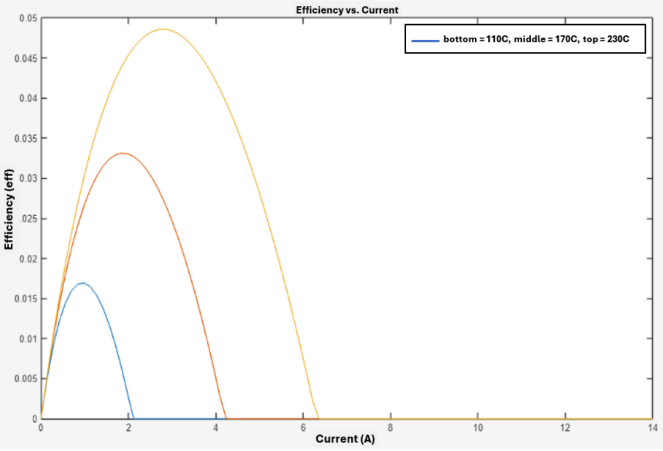

Figure 8. Efficiency as a function of current for baseline TEG leg.

Reconfigured Composite Leg Solution

In an effort to understand the effects of voids in the TEG element with respect to structural displacement behavior and power generation, Mativo et al. (2021) studied volume fraction of the base material from 100% and stopped at 40% where structural instability occurred. Table 1 presents the structural design parameters.

Table 1. Structural design parameters (Mativo, 2020).

Design parameter	Quantity
Design domain	60 units in the *x* direction
	20 units in the *y* direction
Fixed void region	20 units in the *x* direction
	16 units in the *y* direction
Leg height	16 mm
Leg cross-sectional area	400 mm
Bismuth telluride density	7.8587 g cm^{-3}
Bismuth telluride Young's modulus	8.1 – 50 GPa
Bismuth telluride ultimate tensile strength	7.4 GPa
Bismuth telluride density	7.37 g/cm^3
Bismuth telluride melting point	585°C
Bismuth telluride Seebeck coefficient, α_p, α_n	0.000215, -0.000215 v K^{-1}
Bismuth telluride thermal conductivity, k_p, k_n	1.47 Wm^{-1} K^{-1}
Temperature—heat source	110°C < T ≤ 230°C
Temperature—heat sink	50°C
Poisson's ratio	0.23

Table 2 depicts various volume fractions that illustrate reconfigured models. The reconfigured TEG legs in this study occupied approximately 70% of the total baseline area. This percentage maintained the integrity of the structure as thermal load was applied. Beyond this percentage, the legs became unstable and were unable to hold the applied mechanical loading. The reconfigured design depicts the top of each leg with void regions and less material creating connectivity to the top cover which allowed flexibility induced by shear loading. While the design increased TEG flexibility, it also introduced barriers to heat paths caused by the voids. Figures 9 and 10 show how the authors overcame this barrier by using a conducting polymer, PEDOT:PSS, without additional thermal restrictions, because of the similar thermal conductivity of the two materials (Faghani, 2010; Zhang, Sun, Katz, Fang & Opila, 2010; Song et al., 2013; Liu, Wang, Li, Coates, Segalman & Cahill, 2015). When selecting material properties for the TEG, tradeoffs between thermal conductivity and electrical resistivity were considered (LeBlanc, 2014). Filling the voids transformed the leg into a reconfigured composite TEG leg and removed the thermal flow restriction that would have required higher temperatures to enable convection and radiation, respectively, to expand the heat path.

Table 2. Displacement, power, and shape of an integrated TEG for the vibratory environment (Mativo et al., 2021).

Volume fraction	Displacement (%)	Power generation at 230°C (W/mK)	Shape
100	5.04	1.0499	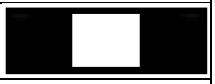
90	5.55	0.9725	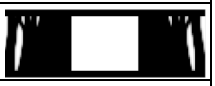
80	6.36	0.8937	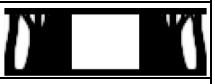
70	7.84	0.8115	
60	10.31	0.7264	
50	12.90	0.6374	
40	14.20	0.5313	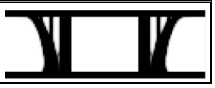

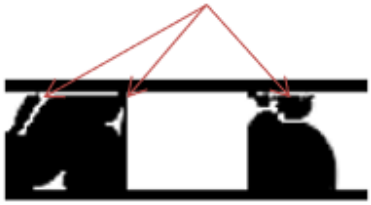

Figure 9. Topology of an optimal TEG unit cell indicating where PEDOT:PSS was applied.

Figure 10. Reconfigured composite TEG unit cell.

As a polymer, PEDOT:PSS does not interfere with the flexibility of the reconfigured TEG leg. It was assumed that the interface between the Be_2Ti_3 and PEDOT:PSS would have no effect on the calculation of power and efficiency of the reconfigured leg. Figure 10 shows the interface. The new bismuth telluride and PEDOT:PSS reconfigured

composite TEG legs of Figure 10 provided both flexibility and an enhanced heat transfer path for the temperatures used in this study. Various heat source temperatures (e.g., 230°C, 170°C, and 110°C) were applied across the heat plate at different times, and a heat sink of 50°C was set. The reconfigured composite TEG leg model was subjected to the temperature gradients at equal intervals. Figure 11 shows power as a function of current behaving in a parabolic manner. It follows that a higher temperature input resulted in a higher power. The line graphs represent 60°C increments from 110-230°C. The temperature at the heat sink was maintained at 50°C. Following the baseline graph, Figure 12 shows a higher efficiency.

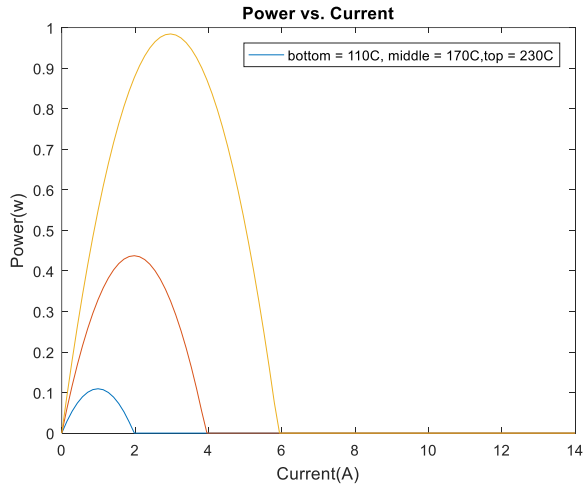

Figure 11. Output power as a function of electrical current for a TEG reconfigured composite leg.

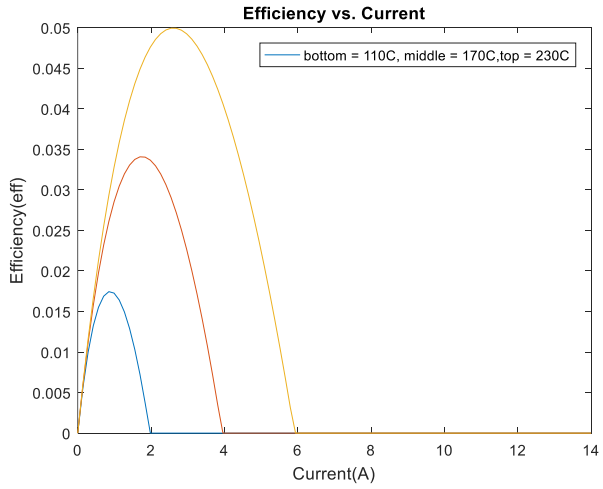

Figure 12. Efficiency as a function of current for a reconfigured composite TEG leg.

The power output generated by the reconfigured composite leg was slightly below (94%) the baseline. Table 3 shows an overall power generation comparison between the baseline and the reconfigured composite models. Table 4 shows that the reconfigured composite leg had a 3% increase in efficiency.

Table 3. Maximum power generation for the two models.

Experiment/ Temperature	Baseline (W/mK)	Reconfigured - Composite (W/mK)
230°C	1.0499	0.9844
170°C	0.4667	0.4375
110°C	0.1163	0.1094

Table 4. Maximum efficiency for the two models.

Experiment/ Temperature	Baseline (%)	Reconfigured - Composite (%)
230°C	4.85	4.99
170°C	3.31	3.41
110°C	1.69	1.74

The power decrease and efficiency increase shown in Tables 3 and 4 were influenced by the change in the composition of the TEG leg with bismuth telluride at 70%, while holding PEDOT:PSS at 30%. In studying the effects of power and electrical resistivity of the reconfigured composite, it was determined that power generated from higher temperature was more impacted than from lower temperatures. Figure 13 shows how this can be caused by the higher difference in temperature gradient.

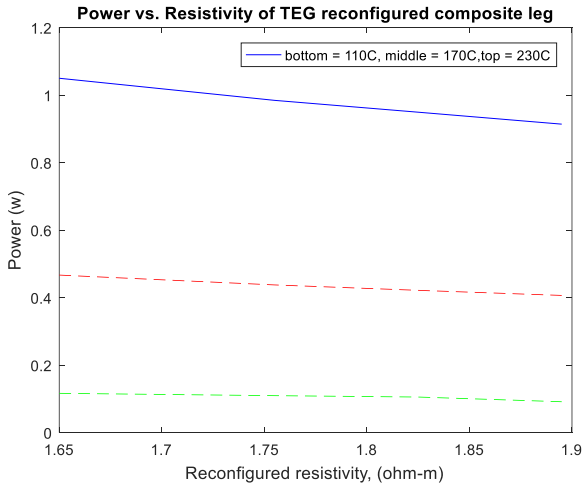

Figure 13. Power decreases in the reconfigured composite TEG leg.

Interestingly, Figure 14 indicates that this study of efficiency and resistivity of a reconfigured composite leg had an increase in efficiency across all input temperatures, with all temperatures assuming the same proportional increase.

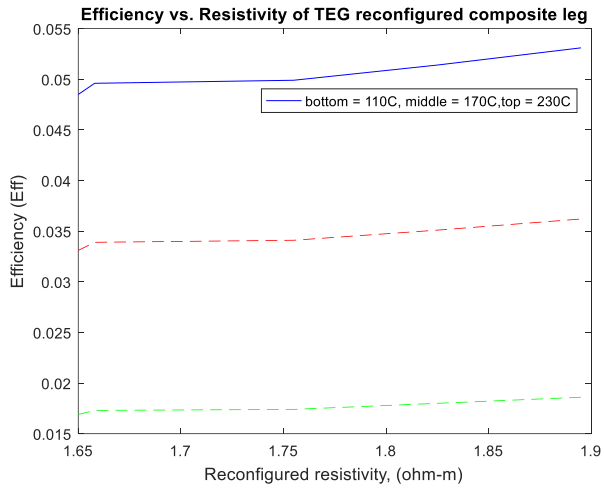

Figure 14. Increase in efficiency for the reconfigured composite TEG leg.

Discussion

Three models were examined in this study. The first model was developed to verify the MATLAB tool for accuracy of the studies to follow. The second experiment studied the baseline model. Results reflected what the Marlow TG12-6 data sheet contained. All models withstood the compression loads specified for the baseline model. The baseline model failed when shear load was applied to it. It was rigid, yet generated the most power per unit cell. The reconfigured composite model generated power at 94% of the baseline model and withstood half of the applied shear load when compared to the baseline model (Mativo, 2020). It should be noted that all experiments in this study were simulations. It is believed that scholarly environments with physical facilities that can build and test the TEG could do so and verify these findings.

The findings from this study suggest that a reconfigured composite TEG leg with a uniform cross-sectional area can safely operate in a vibratory environment. Reconfigured composite TEG legs indicates that both flexibility and thermal conductivity can be achieved by careful structural design and filler material selection. The authors sought to minimize the difference between Bi_2Te_3 and the conducting polymer to fill void regions in the reconfigured design, and PEDOT:PSS was the closest choice. The small difference in the two materials resulted in slightly less power and higher efficiency, when compared to the reconfigured void model. The result was influenced by the polymer path, as opposed to no path (void). The Seebeck effect and thermal conductivity significantly influenced the final outcomes.

Conclusions

The authors attempted to determine the effects of a reconfigured leg on power generation and efficiency. Using the original rectangular legs as a baseline for the study, the authors found that, even though both leg models occupied the same amount of space, the reconfigured leg used about 30% less bismuth telluride. The reconfigured composite TEG leg incorporated PEDOT:PSS to fill the void regions and its power and efficiency results were close to the baseline while adding flexibility, which was the impetus for the original study. It is worth noting that scalability was not considered for this experiment. The assumption was that the mechanical and electrical aspects of the reconfigured TEG model would yield an overall gain of flexibility with minimum power generation loss.

The new reconfigured composite TEG leg is beneficial, as it can provide opportunities to harvest energy in non-planar and vibratory environments. A tradeoff of slightly reduced overall power generation (6%) compared to no access to free waste energy in vibratory environments is worth consideration. Many waste heat-emitting sources such as engines, boilers, bridges, and vehicles are vibratory in nature and can use the harvested energy to further their missions or run auxiliary systems. Finally, an increase in efficiency is welcome.

References

Baskaran, P., & Rajasekar, M. (2025). Recent Progress in Thermoelectric Devices and Applications. *Chemical Engineering Journal, 506*, January 15, 159929. https://doi.org/10.1016/j.cej.2025.159929

Chen, L., Meng, F., & Sun, F. (2012). Maximum power and efficiency of an irreversible thermoelectric generator with a generalizable heat transfer law. *Scientia Iranica*, *19*(5), 1337-1345.

Faghani, F. (2010). *Thermal Conductivity Measurement of PEDOT:PSS by 3-omege Technique*. Linkoping University.

He, R., Schierning, G., & Nielsch, K. (2018). Thermoelectric Devices: A review of Devices, Architectures, and Contact Optimization. Thermoelectric Devices. *Advanced Materials Technologies, 3*(4), 1700256. https://doi.org/10.1002/admt.201700256

Kanimba, E., & Tian, Z. (2016). Modeling of a Thermoelectric Generator Device. Thermoelectric for Power Generation. In S. Skipidarov, & M. Nikitin (Eds.*), Thermoelectrics for Power Generation - A Look at Trends in the Technolog*. https://doi.org/10.5772/65741

LeBlanc, S. (2014). Thermoelectric generators: Linking material properties and systems engineering for waste heat recovery applications, *Journal of Sustainable Materials and Technologies, 1*(2), 26-35.

Liu, J., Wang, X., Li, D., Coates, N. E., Segalman, R. A., & Cahill, D. G. (2015). Thermal Conductivity and Elastic Constants of PEDOT:PSS with High Electrical Conductivity. *Macromolecules*, *48*(3), 585-591. https://doi.org/10.1021/ma502099t

Marlow Industries. (2015). TG 12-6 Data Sheet. https://www.digikey.com/en/htmldatasheets/production/1958589/0/0/1/tg12-6-datasheet

Mativo, J. M. (2020). *System Design of Composite Thermoelectrics for Aircraft Energy Harvesting* (Unpublished doctoral dissertation). University of Dayton. OhioLINK Electronic Theses and Dissertations Center. http://rave.ohiolink.edu/etdc/view?acc_num=dayton1607959975788155

Mativo, J., Hallinan, K., George, U., Reich, G., & Steininger, R. (2021). Topology optimized thermoelectric generator: a parametric study. *Energy Harvesting and Systems, 7*(2), 33-53. https://doi.org/10.1515/ehs-2021-0002

Olivares-Robles, M. A., Badillo-Ruiz, C. A., & Ruiz-Ortega, P. E. (2020). A comprehensive analysis on nanostructured materials in a thermoelectric microsystem based on geometric shape, segmentation structure and load resistance. *Sci Rep, 10*, 21659. https://doi.org/10.1038/s41598-020-78770-9

Rowe, D. M. (2006). *CRC handbook of thermoelectric: Macro to nano*. Boca Raton, FL: RC. https://www.alibris.com/CRC-Handbook-of-Thermoelectrics/book/1380645

Ruiz-Ortega, P. E., Olivares-Robles, M. A., & Ruiz, A. F. G. (2018). Thermoelectric Cooling: The Thomson Effect in Hybrid Two- Stage Thermoelectric Cooler Systems with Different Leg Geometric Shapes. *IntechOpen*. https://doi.org/10.5772/intechopen.75440

Saqr, K. M., & Musa, M. N. (2009). Critical Review of Thermoelectric in Modern Power Generation Applications. *Thermal Science, 13*(3), 165-74. https://doi.org/10.2298/tsci0903165s

Song, H., Liu, C., Zhu, H., Kong, F., Lu, B., Xu, J. … Zhao, F. (2013). Improved Thermoelectric Performance of Free-Standing PEDOT:PSS/ Bi_2Te_3 Films with Low Thermal Conductivity. *Journal of Electronic Materials, 42*(6), 1268-1274.

Telkes, M. (1947). The efficiency of thermoelectric generators. *International Journal of Applied physics*, *18*, 1116 -1127.

Yang, L., Huh, D., Ning, R., Rapp, V., Zeng, Y., Liu, Y. … Prasher, R. S. (2021). High thermoelectric figure of merit of porous Si nanowires from 300 to 700 K. *Nature Communication, 12*, 3926. https://doi.org/10.1038/s41467-021-24208-3

Zhang, B., Sun, J., Katz., H. E., Fang, F., & Opila, R. L. (2010). Promising Thermoelectric Properties of Commercial PEDOT:PSS Materials and Their Bi_2Te_3 Powder Composites. *American Chemical Society Applied Materials & Interfaces, 2*(11), 3170-3178.

Biography

JOHN M. MATIVO obtained his PhD in mechanical engineering from the University of Dayton, Ohio, and EdD in technical education from the University of Georgia. He is a Josiah Meigs Distinguished Professor at the University of Georgia. His research revolves around both workforce education and energy harvesting. In workforce education, he studies best practices for teaching and learning in STEM fields. In energy harvesting, he develops tools to access waste heat. Dr. Mativo may be reached at jmativo@uga.edu

PAUL A. ASUNDA obtained his PhD from the University of Georgia and is an associate professor of engineering and technology teacher education in the Department of Technology Leadership and Innovation at Purdue University. His research and scholarship focus on supporting integration of engineering design and computational thinking practices in integrated science, technology, engineering and math (i-STEM) disciplines. Dr. Asunda may be reached at pasunda@purdue.edu

Utilizing Machine Learning Multi-Output Regression Methods to Predict Turning Movements at Intersections

Somayeh Nazari Enjedani, Boise State University; Mandar Khanal, Boise State University

Abstract

Traffic signal timing design at intersections requires data on the turning movements (TMs) of vehicles that travel through the intersections. Turning movements at traffic intersections refer to the directional choices that drivers of the vehicles make—left turns, through movements, right turns, and U-turns—as they navigate the intersection. Traditional methods of TM data collection are costly, time-consuming, and do not deliver real-time data. Alternative techniques such as video image processing enable the near-real-time collection of approach volumes and turning movements. However, these methods require expensive, specialized equipment at the intersection. As a result, manual counting has remained the predominant method for collecting TM data at intersections.

In this current study, the authors developed a robust method for collecting TM data. The TM counts, approach volume, intersection type, and lane configuration of 400 intersections around Ada County, Idaho, USA, were analyzed to develop an accurate and reliable turning-movement estimation model. A total of 2400 hours of TM counts were used. Three different machine learning multi-output regression methods were applied to analyze the relationship between the approach volumes and the corresponding turning movements, intersection type, and lane configuration. The results indicated that the developed model had a remarkable capability for accurately forecasting TMs.

Introduction

In order to undertake traffic operational analysis and design studies such as intersection design and signal timing design, transportation engineers and planners need accurate turning-movement counts at intersections (Noyce, Bill, Chitturi & Santiago-Chaparro, 2019). It is not costly or complicated to collect approach volumes using existing vehicle detection infrastructure. Loop detectors, microwave detectors, and video-imaging detectors are all examples of stationary sensors that have long been employed to count approach volumes (Vigos & Papageorgiou, 2010). These devices are capable of measuring approach volumes, but they are unable to measure TMs. TMs are the categorization of an approach traffic stream into left, right, and through streams that pass through the intersection (Karapetrovic & Martin, 2021). Numerous researchers have made efforts to suggest novel ways to calculate TMs from approach volumes, but none has been found to be effective enough for use in the U.S. Many of the proposed methods require special equipment that is expensive to install or has a limited scope of use. For example, they may not work when there is a shared lane. Currently, manual counting remains the most common approach for collecting TM data, even though there are several drawbacks to it. There are several issues that arise while collecting TMs through manual counts. Manual counting is a tedious and time-consuming method representing snapshots in time; as such, it is unable to provide traffic data in real-time or on a continuous basis, which is necessary for gaining insight into how traffic patterns change over time (Ghods & Fu, 2014). Replacing manual traffic counting with superior techniques can provide more accurate, efficient, and comprehensive data on traffic flow, which can help city planners and traffic engineers make better decisions about traffic management and infrastructure improvements.

The estimation of future traffic confronts transportation engineers and planners with an additional challenge. Turning movements are typically approximated using the origin-destination (O-D) matrix, when traffic agencies forecast future traffic for existing or planned traffic networks. The O-D matrix thereafter undergoes iterative operations to achieve equilibrium in the turning movements (Project Traffic Forecasting Handbook, 2014). While this methodology is frequently used and acknowledged as a conventional procedure, constructing the origin-destination matrix requires comprehensive surveys and is contingent upon varying land-use assumptions. Consequently, it is essential to revise the O-D matrix in response to any changes in the adjacent land use. Furthermore, in instances where the traffic network is of limited scale, such as in the scenario of an isolated intersection, the practicality of using an O-D matrix is questionable. In light of the aforementioned limitations, it is essential to explore other approaches for calculating TMs.

This study departs from the conventional methodology that relies on a predefined set of assumptions and iterative adjustments to attain a balance between inbound and outbound traffic. Instead, a machine learning (ML) approach was adopted that focused on understanding the intricate relationships between approach volumes, turning movements, and various traffic and geometric attributes of intersections. These insights were then utilized to develop predictive models. ML methods, a subset of artificial intelligence, empower computers to autonomously learn and make predictions or decisions without explicit task-specific programming. They discern patterns within the data and

subsequently employ these patterns to make informed decisions. Furthermore, ML methods possess the capability to extend predictions to unseen data, based on patterns gleaned from existing data sources. In this current study, the authors took advantage of ML methods to solve the problem of TM counts at intersections.

This research entailed the training of ML techniques on manual count data to meticulously investigate the relationship between approach volumes and the corresponding turning movements, as well as two other key features of intersections. A number of earlier studies also attempted to find the relationship between turning movements and approach volumes with the aid of ML approaches. In this current study, however, the authors aimed to enhance previous research by including more crucial intersection features in the predictive variables of the model. These additive predictive variables were descriptive variables, as opposed to approach volumes that are numerical variables. Using a combination of numerical and descriptive variables as predictive variables helps to capture a broader range of relationships in the data. The two descriptive data items applied in this study gave more information about the lane configuration of approaches and the type of intersection.

For this study, manual count information and geographic data from around 400 intersections in Ada County, Idaho, were collected and encompassed 1242 manual count data sheets. Additionally, a detailed database on lane configuration for each approach at every intersection and intersection type was generated. The results from applying ML models to the final data frame revealed that the proposed approach has the potential to serve as a robust platform for the utilization of the available manual count of approach volume data to estimate TMs at intersections. It can, then, contribute significantly to intersection and signal timing design for intersections and can either fill data gaps in current situations or make predictions for future intersections where data are scarce or nonexistent.

Literature Review: Materials and Methods

Researchers have long endeavored to find an alternative technique to replace manual counts. They attempted to calculate TM data by utilizing the origin-destination (O-D) matrix, but this strategy proved to be imprecise and unstable. O-D matrices are often used in transportation planning as a means of aggregating data to show the overall number of trips between certain zones or places. The provided information lacks specificity on the movement patterns of vehicles inside designated areas, especially within intersections. To solve the problem, these methods consider some unrealistic assumptions that make the results inaccurate. Besides, these methods are not able to give real-time TM data (Nihan & Davis, 1989; Pratelli, Sordi & Farina, 2021). Several researchers have tried to develop mathematical algorithms that can use data obtained by detectors to determine the TMs of vehicles based on approach volumes. These methods, however, have always been severely constrained. For example, some of them were inapplicable to intersections with shared lanes or those that did not have a simple geometry (Hauer, Pagitsas & Shin, 1981; Maher, 1984; Mahmoud, Abdel-Aty, Cai & Yuan., 2021; Noyce, Chittori, Santiago-Chaparro & Bill, n.d.; Virkler & Kumar, 1998).

A number of other researchers attempted to determine TMs by analyzing the data obtained from pre-existing video detection systems installed at signalized intersections (Shirazi & Morris, 2016; Yi & Zhang, 2017; Shirazi & Morris, 2014; Bélisle, Saunier, Bilodeau & Le Digabel, 2017). Yet others proposed methodologies for intersections equipped with radar-based, vehicle-detection systems (Santiago-Chaparro, Chitturi, Bill & Noyce, 2016). Although some of these methods were successful, one primary concern associated with these methodologies was the limited versatility of video detection devices or radar-based sensors, resulting in a limited number of potential uses of these systems. Furthermore, all of these techniques incurred significant costs, due to the need to deploy specific equipment at the intersections. The advent of connected vehicles (CVs) opened up several opportunities for improving the operation of traffic signals. It encouraged some researchers to use CV data to aid in estimating TMs. What prevents these methodologies from becoming practical is the low penetration rate of CV data. The assumed penetration rate in these studies was much higher than the real penetration rate (Saldivar-Carranza, Li & Bullock, 2021; Saldivar-Carranza, 2021). Still other researchers attempted to address this problem, but CV data were still not free at the time, and organizations were required to pay for it (Zheng & Liu, 2017; Nazari Enjedani & Khanal, 2023).

Alternatively, a number of scientists have attempted to model TM counts at intersections using machine learning methods. In one study, the authors proposed a method for estimation of TMs based on approach volumes using an artificial neural network (ANN). This method relies on understanding the underlying relationships between the approach volumes and the TMs, and then using these relationships to make predictions (Ghanim & Shaaban, 2019). In another attempt of applying ML methods to solve the TM problem, machine learning-based regression models, including Random Forest Regressor (RFR), multi-output regressor (MOR), and an artificial neural network (ANN) model, were developed and trained to analyze the relationship between approach volumes and corresponding turning movements (Shaaban, Hamdi, Ghanim & Shaban, 2022). What distinguishes these models is their singular focus on the correlation between approach volume and turning movements (TMs). Remarkably, they do not consider the geometric details or any other distinctive intersection features in their computations. However, it is important to acknowledge that TM is influenced by factors beyond approach volumes.

In this current study, the authors endeavored to pioneer a more comprehensive approach by crafting a multi-output

TM regression ML model. The innovative model described in this paper delves into the intricate web of relationships between approach volumes, intersection types, lane configurations, and the corresponding turning movements. The goal was to provide a holistic understanding of how these multi-faceted factors collectively influence vehicular movements at intersections.

ML-Based, Multi-Target Regression Models for Predicting Turning Movements

The purpose of this research project was to create and assess ML-based, multi-target regression models for estimating TMs at signalized intersections. When there is a scarcity of traffic data, or TM counts, the benefits of such models become readily apparent. In particular, when only approach volumes (either actual or forecast) are provided, the proposed models would create dependable and effective TMs. The multi-target regression models convey the relationship between the approach volumes, intersection classification, lane configuration, and the corresponding turning movements. After developing the turning movement models, predicting turning movement volumes from approach volumes becomes possible and practicable. When working with planning data or newly planned intersections, the use of such models becomes even more valuable.

Figure 1 depicts a typical four-legged intersection. There are three potential TMs for each approach: right, through, and left. U-turns are added to left-turns. The goal of this current research project was to estimate a total of 12 potential TMs for a regular four-approach intersection. The authors considered a turn from approach i to approach j, as T_{ij}. Furthermore, there were four inbound volumes denoted as In_i and four outbound volumes denoted as Out_j; their values were obtained from detector data using Equations 1 and 2. As the equations show, there were eight constraints for a four-legged intersection.

$$In_i = \sum_j T_{ij} \left(i = 1,2,3,4; j = 1,2,3,4; j \neq i \right) \quad (1)$$

$$Out_j = \sum_i T_{ij} \left(j = 1,2,3,4; i = 1,2,3,4; i \neq j \right) \quad (2)$$

It should be noted that only seven of these equations were independent, since the eighth could be expressed as a function of the first seven. This characterization would then be used to choose the independent variables for the model. With 12 TMs (T_{ij}) and only seven equations, it is clear that there were many possible solutions, and additional information had to be provided in order to obtain a unique set of estimates for T_{ij}. In this study, this issue was handled by treating the problem as a multi-target regression problem. In a single-target variable regression problem, there is one input (or feature) vector and one corresponding target variable needs to be predicted. In a multi-target regression problem, there are multiple target variables that must be predicted simultaneously. The target variables here are the counts of left, through, and right turns (T_{ij} in Figure 1) for each observation, which is each approach of an intersection for a specific hour; this means that there was more than one target variable for each observation in the dataset. Since the goal was to predict multiple numerical or continuous target variables simultaneously, which were traffic counts, the problem was a multi-output regression problem.

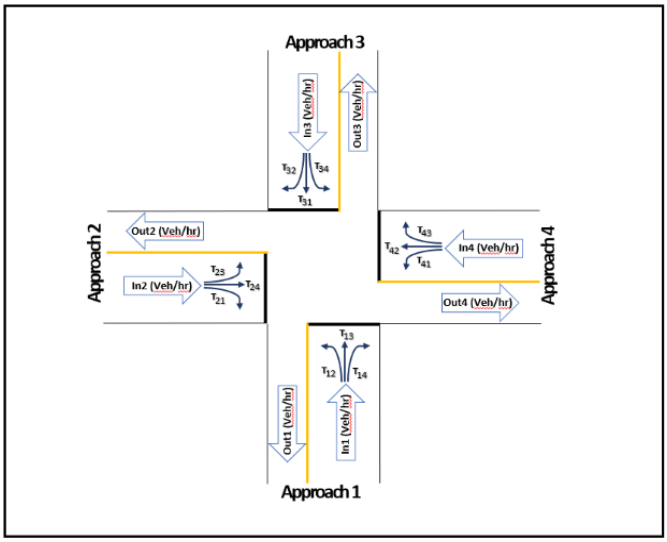

Figure 1. Graphical illustration of TMs at a four-legged signalized intersection.

As mentioned previously, one-hour traffic counts on an approach to each intersection were considered an observation in this model. Each observation had three target variables, which were three TMs of an approach. For example, in Figure 1, which depicts a four-legged intersection, for approach 1, these target variables were T_{12}, T_{13}, and T_{14}. Each observation also needed a number of predictive variables to make the model work. The predictive variables included all approach volumes at an intersection, plus some other functional and geometrical properties of the intersection. The inbound and outbound traffic volumes on all approaches at each intersection made up eight columns of predictive variable data. These eight predictive variables for approach 1 in Figure 1 were In1, In2, In3, In4, Out1, Out2, Out3, and Out4. A clockwise scheme was used while filling up the data table. In1 and Out1 were the inbound and outbound volumes of a given approach. In2 and Out2 were then the inbound and outbound volumes of the approach on the left side of the subject approach. In3 and Out3 were the inbound and outbound volumes of the approach in front of the subject approach. And, finally, In4 and Out4 were the inbound and outbound volumes on the right side of the subject approach. Two additional data items were added that were not numerical variables, such as those in the first group, but were descriptive variables.

Using a combination of numerical and descriptive variables as predictive variables helped to capture different aspects of the problem and improve the predictive power of the model. It further allowed for the capture of a broader range of information and relationships in the data, leading to more accurate and meaningful predictions. The two data items chosen to provide more information to the model were the lane configurations of each approach and the type of intersection. Regarding lane configuration, through a comprehensive analysis, the number of exclusive left-turn lanes was chosen as the lane configuration property of each approach. There could be zero, one, or two exclusive left turns. The "intersection type" was defined as the class of the approach with the highest functional class. There were five distinct classes of approaches in the dataset: local, collector, minor arterial, primary arterial, and expressway. For example, if an intersection included approaches classified as collector, minor arterial, and principal arterial, this intersection would be classified as principal arterial. All observations at this intersection would then have "principal arterial" under the column "intersection type" in the data table.

In summary, a dataset was created with ten predictor variables and three output variables, which were TMs, for each approach. The final step was modeling. Due to the characteristics of the data, this would be considered a multi-output regression problem. The problem was resolved through the implementation of several ML regression models. In this study, to address this issue, Random Forest Regressor (RFR), XGBoost Regressor and Extra Trees Regressor were implemented.

Data Collection and Preparation

The data utilized to construct the models in this study consisted of 1242 TM manual counts obtained from intersections in Ada County, Idaho, from 2017 to 2022. The Ada County Highway District (ACHD) collects manual count data over time and saves it in its database for future use. The manual count data were saved as PetraPro_Datafiles, which were exported into *Excel* format for the purpose of this study. Table 1 presents the annual number of manual counts performed by ACHD in Ada County during the analysis period of this study.

Table 1. Annual number of manual TM counts in Ada County.

Year	Number of Counts
2017	367
2018	294
2019	167
2020	161
2021	50
2022	203
Total	1242

Table 2 shows an illustration of a manual count data *Excel* sheet obtained from ACHD. In addition to columns labeled Left, Thru, and Right, which represent three standard TMs at an approach, there is also a Peds column representing pedestrian movements for each approach with all values zero in Table 2. This is because ACHD does not routinely collect pedestrian data unless a special request is made for them. Based on the requests from designers or planners, survey personnel were deployed to the intersection to record passing vehicles and the turns they made. It can be said that the most common application of manual count data is signal timing design. The TM counts were collected for three peak periods: morning, noon, and evening, which are typically used for traffic operations analysis. Not all the intersections in the database have manual counts for all three distinct peak hours; certain intersections have counts for just one or two peak periods.

The available database pertains to around 400 intersections, which include intersections with three legs, four legs, and more than four legs. There were only a few intersections with more than four legs but were excluded to simplify the model. To apply ML models to these data, the data in these 1242 *Excel* files needed to be organized into one data frame. This final data frame was utilized for subsequent data analysis and modeling purposes. Table 3, containing 9936 rows of data, shows a sample of the final dataset. The first 14 columns of this data frame were built by stacking the manual count data sheets. It is apparent from Table 3 that, for each hour of traffic counting at each approach to each intersection, there is a row of data in the final data frame. Considering the first row of this table, the figures for the Left, Thru, and Right columns come from simply summing up one hour of left turn, through, and right turn manual count data in Table 2. In1 through In4 as well as Out1 through Out4 were calculated according to Equations 1 and 2. These were in-bound and out-bound approach volumes at each intersection.

Each *Excel* sheet of the manual count of a four-legged intersection can contribute to building up eight rows in the final data frame. Manual counts are normally done for two hours around peak hours in the morning, noon, or evening. The aim here was to make the dataset for hourly volumes. Accordingly, it was possible to generate two rows of observations for each approach; having four approaches in a four-legged intersection yielded eight observations from each *Excel* sheet. This procedure was also applied to three-legged intersections; the only difference was that a leg with zero volume would be added to each three-legged intersection. It should be noted that real-time approach volumes are also often available, because detectors are constantly collecting them. Regarding the column Intersection Type, first the street classification of approaches to intersections was requested from ACHD. Table 4 shows a sample of the data frame obtained from ACHD, which has 392 rows; each row represents an intersection and contains the classification of the approaches to that intersection.

Table 2. Example of a manual count sheet.

1	File Name:	S:\Traffic Count Data\Turn Counts\2022\Chateau & Locust Grove PM.ppd															
2	Start Date:	10/11/2022															
3	Start Time:	4:00:00 PM															
4	Site Code:	00000000															
5	Comment 1:	Operator: D White															
6	Comment 2:	Video NEC															
7	Comment 3:																
8	Comment 4:																
9		Locust Grove from Ustick From North					Chateau from Lochness From East				Locust Grove from Fairview From South				Chateau from Jericho From West			
10	Start Time	Left	Thru	Right	Peds	Left	Thru	Right	Peds	Left	Thru	Right	Peds	Left	Thru	Right	Peds
11	4:00:00 PM	0	58	2	0	6	2	8	0	5	80	6	0	8	2	11	0
12	4:05:00 PM	0	66	2	0	5	4	6	0	8	78	4	0	7	2	11	0
13	4:10:00 PM	0	64	1	0	5	1	0	0	3	91	1	0	9	2	6	0
14	4:15:00 PM	0	57	0	0	4	0	3	0	4	80	8	0	3	1	4	0
15	4:20:00 PM	2	58	3	0	7	0	2	0	6	98	4	0	3	0	7	0
16	4:25:00 PM	1	69	2	0	4	0	1	0	6	81	6	0	2	0	6	0
17	4:30:00 PM	2	56	3	0	3	0	0	0	3	79	5	0	3	2	7	0
18	4:35:00 PM	2	67	2	0	14	0	3	0	7	83	8	0	4	0	6	0
19	4:40:00 PM	2	51	2	0	3	0	2	0	9	100	4	0	3	0	3	0
20	4:45:00 PM	1	78	3	0	5	0	4	0	8	68	6	0	1	1	2	0
21	4:50:00 PM	0	52	4	0	5	0	5	0	6	79	10	0	3	1	5	0
22	4:55:00 PM	3	56	4	0	2	1	4	0	5	91	10	0	2	0	4	0
23	5:00:00 PM	0	54	4	0	7	0	2	0	10	72	5	0	3	2	5	0
24	5:05:00 PM	1	58	4	0	8	0	1	0	7	78	6	0	3	3	5	0
25	5:10:00 PM	0	53	3	0	3	0	3	0	5	89	4	0	6	2	6	0
26	5:15:00 PM	1	74	1	0	1	1	0	0	3	96	5	0	3	1	4	0
27	5:20:00 PM	1	79	4	0	3	1	2	0	4	115	3	0	3	0	2	0
28	5:25:00 PM	0	61	1	0	3	0	2	0	15	72	5	0	3	1	3	0
29	5:30:00 PM	1	69	2	0	3	0	4	0	5	101	5	0	4	0	1	0
30	5:35:00 PM	1	73	1	0	6	0	3	0	7	88	1	0	6	1	6	0
31	5:40:00 PM	1	57	1	0	3	0	0	0	7	89	4	0	4	1	3	0
32	5:45:00 PM	1	61	4	0	3	0	1	0	6	89	3	0	2	0	3	0
33	5:50:00 PM	0	69	2	0	1	0	4	0	5	90	4	0	6	1	4	0
34	5:55:00 PM	3	48	5	0	3	0	0	0	4	81	2	0	1	0	4	0

The approach with the highest functional class was selected as the intersection type and that was used to fill the column Intersection Type in Table 3 for each approach. For lane configuration, the aim was to collect the number of lanes and their functionality for each approach in the analysis. As no database for lane configuration data from ACHD or other transportation authorities in Idaho could be found, Google Maps was used to collect these data manually. Table 5 shows a sample of the collected lane configuration data frame. This data frame has around 1600 rows. Lane configuration data provide the number of lanes of each type in each approach. Exclusive left shared left and through, through, shared left, through and right, shared through and right, exclusive right, and shared left and right encompass the types of lane configurations. After investigating these data and to limit the number of independent variables, the decision was made to apply only the number of exclusive left lanes as the lane configuration characteristic.

The number of exclusive left lanes was picked, because there was more variation among intersections in this lane type compared to other lane types, making it more informative for the model. The number of exclusive left turn lanes was found to be zero, one, or two. Accordingly, the column, lane configuration, in Table 3 was populated with the number of exclusive left lanes for each approach. Figure 2 shows a correlation matrix that was developed for the input data attributes and the output variables.

In Figure 2, the rows and columns labeled "in," "in-left," "in-opp," and "in-right" correspond to columns In1, In2, In3, and In4 in Table 3, respectively. Similarly, the rows and columns labeled "out," "out-left," "out-opp," and "out-right" correspond to columns Out1, Out2, Out3, and Out4 in Table 3, respectively. Multiple interesting relationships can be seen in Figure 2 that could have a powerful impact on regression results. For example, the output Thru is correlated positively with the inputs In and out-opp. After preparing the dataset, the next step was modeling the data with the help of machine learning methods to find the underlying relationship between TMs with approach volumes, intersection type, and lane configuration.

Multi-Output Regression Models

The prepared dataset represents a multi-output regression problem, since it has multiple target variables. This model has three continuous outputs, which are the three TM counts. Several machine learning models can be used for modeling multi-output regression datasets. Among them, RFR, XGB Regressor, and Extra Trees Regressor were selected for use in this current study. These multi-output regression models were applied to predict the TM counts at signalized intersections. Figure 3 summarizes the procedure. These three different ML techniques for multi-output regression were applied to the dataset under two different scenarios, and their outcomes were compared and assessed.

Table 3. A sample of a final database.

Intersection	Approach	Left	Thru	Right	In1	In2	In3	In4	Out1	Out2	Out3	Out4	Int Type	Lane Configuration
Chateau & Locust Grove PM	Locust Grove from Ustick from North	13	732	28	773	109	1150	131	1094	96	867	106	*M	1
Chateau & Locust Grove PM	Chateau from Lochness from East	63	8	38	109	1150	131	773	96	867	106	1094	*M	0
Chateau & Locust Grove PM	Locust Grove from Fairview from South	70	1008	72	1150	131	773	109	867	106	1094	96	*M	1
Chateau & Locust Grove PM	Chateau from Jericho from West	48	11	72	131	773	109	1150	106	1094	96	867	*M	0

*Minor Arterial

Table 4. A sample of an approach classification data frame.

Name of Intersection	Approach 1	Approach 2	Approach 3
16th & Hays	Minor Arterial	Minor Arterial	
16th & Idaho	Minor Arterial	Collector	
16th & Washington	Minor Arterial	Collector	
26th, 27th & State	Minor Arterial	Collector	Principal Arterial
27th & Main	Collector	Principal Arterial	
28th & Heron	Collector	Local	
28th, 29th & State	Collector	Local	Principal Arterial
31st, State & Whitewater Park	Local	Principal Arterial	Minor Arterial
33rd & State	Local	Principal Arterial	
36th, Chinden & Orchard	Collector	Principal Arterial	Principal Arterial

Table 5. A sample of a lane configuration data frame.

Name of Intersection	Name of Approach	Exclusive Left	Left +Thro	Thro	Left + Thro + Right	Thro + Right	Exclusive Right	Left + Right
Chateau & Locust Grove	Locust Grove from Ustick from North	1	0	0	0	1	0	0
Chateau & Locust Grove	Chateau from Lochness from East	0	0	0	1	0	0	0
Chateau & Locust Grove	Locust Grove from Fairview from South	1	0	0	0	1	0	0
Chateau & Locust Grove	Chateau from Jericho from West	0	0	0	1	0	0	0
Fairview & Locust Grove	Locust Grove from Ustick from North	1	0	1	0	1	0	0
Locust Grove & McMillan	Locust Grove from Ustick from South	1	0	1	0	0	1	0
Locust Grove & Pine	Locust Grove from Fairview from North	1	0	1	0	1	0	0
Locust Grove & Ustick	Locust Grove from Fairview from South	1	0	1	0	1	0	0

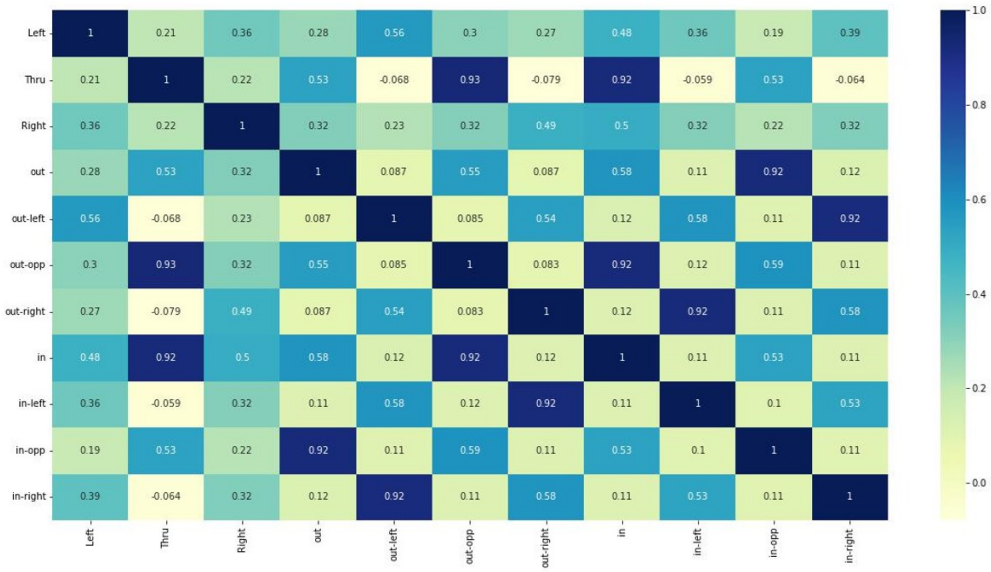

Figure 2. Visualization of the correlation matrix between input and output variables.

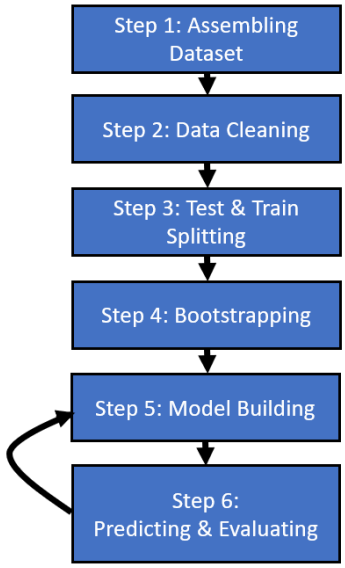

Figure 3. Prediction process.

In Scenario 1, all three target variables and the eight predictive variables were used in their original form, which was traffic counts per hour. There were no data transformations in this scenario. Scenario 2 tried to transform all three target variables and those eight predictive variables that were approach volumes into ratios. In both scenarios, the two remaining predictive variables, Intersection Type and Lane Configuration, were the same and did not undergo any data transformation. The columns Left, Thru, and Right in Table 3 can be replaced with the proportion of the left turn, through, or right turn counts relative to the whole approach volume. The columns In1 to In4 in Table 3 can be replaced with the share of each approach relative to the total entering traffic to the intersection. The same logic was applied to transform the content of columns Out1 to Out4 from traffic counts to ratios.

Figure 3 shows that, after the dataset was assembled, the data cleaning procedure was applied to the data. In this study, the data cleaning procedure involved preprocessing the data by removing outliers. This step was crucial, because the quality of the data directly impacted the performance and reliability of the models. It is common to start by identifying outliers in the predictive variables, because they can directly affect the performance of the model. However, depending on the nature of the problem, the analyst may also want to examine outliers in the target variables, especially if they represent unusual events (Han, Kamber & Pei, n.d.). The specific context and objectives of the analysis or modeling task should ultimately serve as a guide for the decision. Here, outliers were examined only in the predictive variables. The Z-score method, which is a statistical method to find outliers, was chosen to apply to the dataset. This method calculates the Z-score for each data point and identifies those with Z-scores above a certain threshold. Overall, 12 intersections had outliers, and they were deleted from the final database before modeling.

In Figure 3, Step 3 is about forming the training and test datasets. Splitting data into training and test datasets is a fundamental practice in machine learning for evaluating the performance of a model. The purpose of this split is to assess how well the model can generalize to new, unseen data. In other words, a subset of the data is set aside before starting the analysis, and this serves as new, unseen data in the evaluation process. Test-train split aids in model evaluation, preventing overfitting, parameter tuning, assessing generalization, and avoiding data leakage. By training the model on the training set and then evaluating its performance on another independent portion that is the test dataset, it is possible to simulate how the model will perform in the real world when it encounters new, unseen examples (Mueller & Guido, 2016). In this study, the dataset was divided into 20% and 80% for test and training purposes, respectively. It indicates that the model was developed with 80% of the data and then evaluated for performance on 20% percent of the unseen data.

The following step in Figure 3 is the bootstrapping procedure. It involves repeatedly sampling the original dataset with replacement. The purpose of bootstrapping is to create multiple resampled datasets from the original training data, each of which can be used to train a different instance of the model. Bootstrapping is typically performed on the training data when working with machine learning models. The primary reason for bootstrapping on the training data is to introduce diversity and reduce overfitting in the model. By repeatedly sampling with replacement from the training data

to create different training subsets, variations would be generated in the training process. This helps the model learn different aspects of the data and become more robust, improving its generalization to unseen data. Bootstrapping is typically not performed on the entire dataset. The test data should remain independent of the training process and represent unseen examples. Bootstrapping on the test data would introduce bias and invalidate the assessment of model performance on new, unseen data. That is why the bootstrapping step occurs after the training-test split (Alpaydin, 2020). The next step is to apply the modeling procedure on the training dataset. As mentioned earlier, three different ML techniques for multi-output regression, including Random Forest Regressor (RFR), XGB Regressor, and Extra Trees Regressor, were applied to the dataset. The programming language Python was used to implement, train, and evaluate the models.

Random Forest Regressor (RFR)

An RFR is a machine learning model that falls under the category of ensemble learning and is used for regression tasks. It is an extension of the Random Forest algorithm, which was originally designed for classification but can also be applied to regression problems (Vanderplas, 2016). Random Forest starts by creating multiple subsets of the original dataset through a process called bootstrapping (with replacement). This means that, for each subset, some data points will be repeated, while others may be left out. These subsets are used to train individual decision trees. At each node of a decision tree, Random Forest randomly selects a subset of features from the entire feature set. Earlier, different features of this study were discussed, including 10 predictive variables that were collected in the dataset. This feature selection process introduces diversity among the trees and helps prevent overfitting. Each subset of the data is used to train a decision tree independently. These trees are typically shallow; they are not allowed to grow very deep. This restriction helps maintain the diversity among the trees and reduces the risk of overfitting.

In the case of regression (predicting continuous values), the final prediction is obtained by averaging the predictions of all the individual decision trees. The individual decision trees, which have been trained on different subsets of the data with different features, are combined into an ensemble. This ensemble approach improves the model's performance and reduces the variance compared to a single decision tree. RFR provides an estimate of its performance without the need for a separate test set known as Out-of-Bag (OOB) Error Estimation. During the bootstrapping process, some data points are not included in the training subset for each tree. These "out-of-bag" data points can be used to estimate the model's accuracy without cross-validation or a separate test set (Segal, 2003). For the purposes of this study, the *RandomForestRegressor* from the *sklearn.ensemble* module and *Multioutput Regressor* from the *sklearn.multioutput* module of the Python library were utilized.

Below is a snippet demonstrating how these libraries were applied to the data frame in this study. X_train and X_test are data frames that contain the training and testing data, respectively. The variables y_pred_train and y_pred_test represent the turning movements predicted by the model for the training and testing data.

```
regr_multirf=MultiOutputRegressor
(RandomForestRegressor
(n_estimators=n1,max_depth=max_depth,
random_state=n2))
regr_multirf.fit(X_train, Y_train)
y_pred_train = regr_multirf.predict(X_train)
y_pred_test = regr_multirf.predict(X_test)
```

Prior to fitting the Random Forest algorithm on the dataset, the maximum tree depth needs to be determined. Maximum depth in a Random Forest algorithm is a crucial hyperparameter that can significantly impact the performance and behavior of the model. It controls the complexity of individual decision trees within the ensemble. It acts as a trade-off between bias and variance in the model. Deeper trees (higher maximum depth) reduce bias but increase variance. Shallower trees (lower maximum depth) reduce variance but may introduce bias. Balancing these trade-offs is crucial for finding a model that generalizes well to new data. Figure 4 shows Mean Squared Error (MSE) versus maximum depth for the RFR on the designed dataset. It seems a maximum depth of 10 would be a good choice in this case, since max depths less than that have a large MSE, and max depths more than that do not help in improving the MSE and only require more computational resources. After deciding on the maximum tree depth, an RFR model was fitted to the dataset.

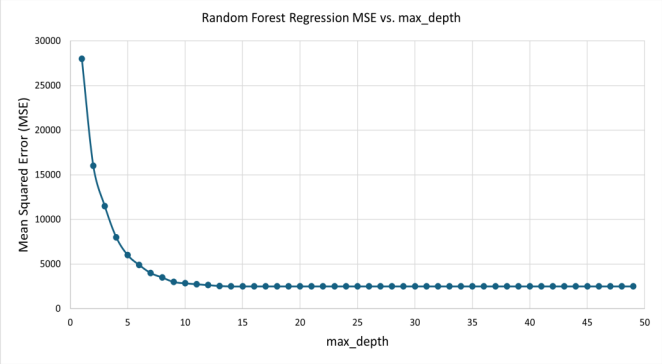

Figure 4. MSE versus maximum depth for Random Forest Regressor.

XGB Regressor

XGBoost (Extreme Gradient Boosting) is a powerful ensemble machine learning algorithm known for its high performance in regression and classification tasks. XGBoost is also an ensemble method that combines multiple decision trees to make predictions. Decision trees are the base learn-

ers used in XGBoost. XGBoost uses a gradient-boosting framework. It builds an ensemble of decision trees sequentially, with each tree aiming to correct the errors of the previous ones. It does this by minimizing a loss function, typically a mean squared error (MSE) loss for regression.

When XGBoost assigns weights to data points, it gives more importance to data points that previous trees incorrectly predicted. This way, it focuses on the most challenging examples, allowing the model to progressively improve its predictions. XGBoost includes L1 (Lasso) and L2 (Ridge) regularization terms to control the complexity of individual trees and prevent overfitting. These regularization terms encourage simplicity and sparsity in the tree structures. XGBoost employs tree pruning to remove branches from the decision trees that do not significantly improve the model's performance. Pruning helps create smaller, more interpretable trees and improves the model's generalization. The learning rate (also called the shrinkage factor) is a hyperparameter that controls the step size in the gradient descent process. It helps determine the contribution of each tree to the final prediction. XGBoost can provide a measure of feature importance, indicating which features have the most influence on the model's predictions. This can be valuable for feature selection and understanding the data. XGBoost is designed for efficiency and can take advantage of parallel and distributed computing. It is capable of handling large datasets and high-dimensional feature spaces. XGBoost can handle missing values in the data by learning the best imputation strategy during training.

XGBoost supports early stopping, allowing for the monitoring of the model's performance on a validation dataset and stop training once the performance starts to degrade. Combining the predictions of all the individual trees yields the final prediction in XGBoost. In regression tasks, this is typically done by averaging the predictions of the trees (Santhanam, Uzir, Raman & Banerjee, 2016). Prior to fitting XGBoost Regressor best values for number of estimators, maximum depth, gamma and learning rate should be determined. Learning rate determines the step size and gamma is a regularization term to control the complexity of the trees. Grid search was applied on the designed dataset to find the optimized values for these parameters. The XGBoost Regressor was then fitted to the dataset. In this study, the *XGBRegressor* from the *xgboost* library, *GridSearchCV* and *KFold* from *sklearn.model_selection*, and *MultiOutputRegressor* from *sklearn.multioutput* of the Python library were employed. Below is a snippet demonstrating how XGBoost was applied to the data frame in this study.

```
XGB_multirf= MultiOutputRegressor(XGBRegressor
(estima-
tor__gamma=0.01,estimator__learning_rate=0.1,estimator
__max_depth=30, estimator__n_estimators=500, ran-
dom_state=2021)) XGB_multirf.fit(X_train, Y_train)
y_pred_train = XGB_multirf.predict(X_train)
y_pred_test = XGB_multirf.predict(X_test)
```

ExtraTrees Regressor

The ExtraTrees Regressor (Extremely Randomized Trees Regressor) is an ensemble machine learning algorithm that uses decision trees to make predictions. However, it has some key differences in its underlying procedure compared to traditional Random Forest. One of the primary differences between ExtraTrees and Random Forest is the way they select features for splitting at each node in the decision trees. In Random Forest, a random subset of features is considered for each node, while in ExtraTrees, all features are considered for each node. This makes ExtraTrees even more random in its feature selection.

Similar to Random Forest, ExtraTrees also uses bootstrapping to create multiple subsets of the training data. Each subset is used to train an individual decision tree. Individual decision trees are trained on these bootstrapped subsets of data, with the primary goal of reducing the variance in the model. The trees are constructed using a random subset of features for each split. In addition to random feature selection, ExtraTrees introduces another level of randomness by selecting the split thresholds at each node in a fully random manner. This differs from Random Forest, which selects thresholds based on a specific criterion such as "Gini impurity" or "mean squared error." Gini impurity is a measure used in decision tree algorithms to evaluate the quality of splits. It helps the algorithm determine the optimal features and thresholds for splitting the data to create a decision tree that best separates the classes in the dataset.

In the case of regression tasks, the final prediction is typically obtained by averaging the predictions from all the individual decision trees. The ensemble of trees provides a robust and accurate prediction by reducing the impact of individual noisy or overfit trees. Like Random Forest, ExtraTrees can handle missing values in the data by considering alternative strategies during the splitting process (Geurts, Ernst & Wehenkel, 2006). The ExtraTrees Regressor was fitted to the dataset as the third method of prediction. In this study, the *ExtraTreesRegressor* from the *sklearn.ensemble* module of the Python library was utilized. Below is a snippet demonstrating how this regressor was applied to the data frame in this study.

```
extra_trees=ExtraTreesRegressor(n_estimators=n1,
max_depth=n2)
extra_trees.fit(X_train,Y_train)
y_pred_train = extra_trees.predict(X_train)
y_pred_test = extra_trees.predict(X_test)
```

Evaluation

In this study, a dataset including three target variables—TMs and a number of predictive variables—was assembled. Subsequently, the dataset was utilized to train multi-target regression models. In order to assess the performance, the observed and predicted turning movements were compared

by computing multiple metrics for each model. The authors used the R^2 score, the mean squared error (MSE), the root mean squared error (RMSE), and the mean absolute percentage error (MAPE) defined in Equations 3-6 to assess the various models developed in this study.

$$R^2 = 1 - \frac{\sum \left(y_{forecast} - y_{actual} \right)^2}{\sum \left(\bar{y} - y_{actual} \right)^2} \quad (3)$$

$$MSE = \frac{\sum \left(y_{forecast} - y_{actual} \right)^2}{N} \quad (4)$$

$$RMSE = \sqrt[2]{\frac{\sum \left(y_{forecast} - y_{actual} \right)^2}{N}} \quad (5)$$

$$MAPE = \frac{1}{N} \sum_1^N \left| \frac{\left(y_{forecast} - y_{actual} \right)}{\left(y_{actual} \right)} \right| \quad (6)$$

The authors also applied the Akaike Information Criterion (AIC) and the Bayesian Information Criterion (BIC) for model selection and comparison during the model-building and evaluation process. AIC is a statistical measure used for model selection and comparison. It balances the goodness of fit of a statistical model to the data with the complexity of the model. AIC quantifies how well a model explains the data, while penalizing models with a higher number of parameters. Lower AIC values indicate models that fit the data well with fewer parameters, making it a valuable tool for choosing the most appropriate model from among a set of candidate models (Forster & Sober, 2011). Equation 7 shows the formulation for AIC:

$$AIC\left(M_k \right) = -2 \log L\left(M_k \right) + 2k \quad (7)$$

where, $L(M_k)$ is the likelihood corresponding to the model M_k and where k is the number of parameters in the model.

BIC is a statistical criterion used for model selection and comparison. Similar to AIC, BIC balances the goodness of fit of a statistical model to the data with the complexity of the model. BIC incorporates a Bayesian perspective by applying a stronger penalty for models with more parameters compared to AIC. It aims to find the model that best explains the data, while favoring simpler models. In practical terms, lower BIC values indicate models that provide a better trade-off between goodness of fit and model complexity, making it a useful tool for selecting the most appropriate model among a set of candidate models (Jordan, Kleinberg & Schölkopf, 2006). Equation 8 shows the formulation for BIC:

$$BIC = -2 * \log L\left(M_k \right) + k \times \log\left(n \right) \quad (8)$$

where, $L(M_k)$ is the likelihood corresponding to the model M_k, k is the number of parameters in the model, and n is the sample size (the number of data points).

To find the best combination of predictive variables for building the final model, six different combinations of predictive variables were initially considered, with RFR applied to each.

- The first combination had six predictive variables, including four inbound volumes (columns In1 through In4 in Table 3), intersection type, and lane configuration.
- The second combination had nine predictive variables, including four inbound volumes (columns In1 through In4 in Table 3) and three outbound volumes (columns Out1 through Out3 in Table 3), intersection type, and lane configuration.
- The third combination had all ten predictive variables, including four inbound volumes (columns In1 through In4 in Table3) and four outbound volumes (columns Out1 through Out4 in Table3), intersection type, and lane configuration.
- The fourth combination had seven predictive variables, including four inbound volumes (columns In1 through In4 in Table 3) and three outbound volumes (columns Out1 through Out3 in Table 3). It did not include intersection type or lane configuration.
- The fifth combination had eight predictive variables, including four inbound volumes (columns In1 through In4 in Table 3) and three outbound volumes (columns Out1 through Out3 in Table 3) and lane configuration.
- The sixth combination had eight predictive variables, including four inbound volumes (columns In1 through In4 in Table3), three outbound volumes (columns Out1 through Out3 in Table3), and intersection type.

Results

Table 6 shows the R^2, MSE, RMSE, MAPE, AIC, and BIC results from applying RFR on these six different combinations to predict TMs. These figures come from predictions on the training dataset. It can be seen that R^2 for all combinations was around 99%, but reliance on the results from training data is not advisable, and the results from test data had to be evaluated. Table 7 shows the R^2, MSE, RMSE, MAPE, AIC, and BIC results coming from applying RFR on the six different combinations to predict TMs using the test dataset. From Table 7, it is evident that the first combination had the lowest R^2; and, its AIC and BIC were comparatively high, so it was set aside. Now, there were five remaining combinations that had R^2 values that were similar, ranging from 91.50% to 93.40%, which

Table 6. Comparison of different predictive variable combinations on the training dataset.

Combination	R^2	MSE	RMSE	MAPE	AIC	BIC
FIRST	99.98%	10	2.86	0.23	191,182	191,238
SECOND	99.96%	15	3.60	0.20	221,935	222,019
THIRD	99.97%	12	3.56	0.18	206,166	206,259
FOURTH	99.96%	15	3.56	0.19	223,195	223,260
FIFTH	99.96%	13	3.00	0.21	213,524	213,599
SIXTH	99.98%	9	2.66	0.15	183,802	183,877

Table 7. Comparison of different predictive variable combinations on the test dataset.

Combination	R^2	MSE	RMSE	MAPE	AIC	BIC
FIRST	80.98%	4217	64.36	88.64	691,465	691,521
SECOND	91.50%	1571	39.43	43.33	600,716	600,800
THIRD	93.40%	1462	37.93	44.38	603,746	603,839
FOURTH	91.99%	1803	42.05	51.49	621,119	621.184
FIFTH	92.29%	2105	45.39	42.75	633,938	634,013
SIXTH	92.77%	1446	37.73	44.63	602,803	634,013

made it hard to decide. However, the primary distinction lay in the fact that the second combination exhibited lower values of AIC and BIC—around 600,716 and 600,800, respectively—on the test dataset, in comparison to the other four combinations. Hence, the second combination was chosen as the model to proceed with for further analyses.

As mentioned previously, the analysis was intended to be conducted under two different scenarios. In Scenario 1, all variables were used in their original form without any transformation. In Scenario 2, variables were transformed into ratios. The goal was to see how converting traffic volumes of each approach to proportions of whole traffic at that intersection would affect the functionality of the model. The process of converting approach traffic volumes to traffic ratios involved the internal relationship between traffic volumes of different approaches at each intersection and the interdependence between TMs of each approach in the model. In these two scenarios, the second predictive variable combination described earlier was used. Combination two, described above, constituted Scenario 1; in Scenario 2, the traffic volumes were converted into ratios. In other words, the target variables, three TMs, were converted to the proportion of each turning movement from the total inbound traffic of that approach. Inbound volumes were converted to the proportion of inbound traffic for each approach from the total inbound traffic to the intersection. Outbound volumes were also converted to ratios of outbound traffic for each approach to the total outbound traffic at that intersection. Table 8 represents an overview of the target variables and predictive variables involved in Scenario 2.

To assess the performance of several multi-output machine learning models on the database, three different ML models, including RFR, XGBoost Regressor, and ExtraTrees Regressor, were applied to the two scenarios. Table 9 represents the outcomes obtained by applying three multi-output machine learning models to two defined scenarios to predict TMs. The figures in Table 9 were derived from predictions on the test dataset. Table 9 shows that Scenario 2 had lower R^2 values for all three ML techniques compared to Scenario 1. Specifically, Scenario 2 had R^2 values of 81.35% for RFR, 82.40% for XGBoost Regressor, and 77.96% for ExtraTrees Regressor, whereas Scenario 1 had R^2 values of 92.50%, 93.99%, and 88.51% for the relevant ML approaches. Converting traffic counts to rates may involve connections between traffic volumes of different approaches at an intersection in the model. However, the investigation demonstrated that this conversion does not improve the accuracy of the model. Hence, the focus was placed on Scenario 1, while Scenario 2 was disregarded.

Another important result that can be extracted from Table 9 is that the XGBoost Regressor outperformed the RFR and Extra Trees Regressor, due to higher values of R^2 and lower values of MSE, RMSE, and MAPE. The R^2 for the XGBoost Regressor was 93.99%, with values of 91.50% for the RFR and 88.51% for the ExtraTrees Regressor. On the other hand, XGBoost Regressor MSE was 1307, while the values for RFR and ExtraTrees Regressor were 1571 and 1997, respectively. Both RMSE and MAPE also followed the same trend. Based on this research, it can be inferred that the most effective model for predicting TMs based on manual counts is the model built on applying the XGBoost Regressor to Scenario 1. Scenario 1 had nine predictive variables, including four inbound volumes (columns In1 through In4 in Table3) and three outbound volumes (columns Out1 through Out3 in Table3), intersection type, and lane configuration.

Table 8. An overview of scenario 2.

Intersection	Approach	Left (%)	Thru (%)	Right (%)	In1 (%)	In2 (%)	In3 (%)	In4 (%)	Out1 (%)	Out2 (%)	Out3 (%)	Int Type	Lane Config
Chateau & Locust Grove PM	Locust Grove from Ustick from North	1.68	94.70	3.62	35.74	5.04	53.17	6.06	50.58	4.44	40.08	*M	1
Chateau & Locust Grove PM	Chateau from Lochness from East	57.80	7.34	34.86	5.04	53.17	6.06	35.74	4.44	40.08	4.90	*M	0
Chateau & Locust Grove PM	Locust Grove from Fairview from South	6.09	87.65	6.26	53.17	6.06	35.74	5.04	40.08	4.90	50.58	*M	1
Chateau & Locust Grove PM	Chateau from Jericho from West	36.64	8.40	54.96	6.06	35.74	5.04	53.17	4.90	50.58	4.44	*M	0

*Minor Arterial

Table 9. Comparison models and scenarios according to R^2, MSE, RMSE, and MAPE.

Model	Scenario1 (%)	Scenario2 (%)	Scenario1	Scenario2 (%)	Scenario1	Scenario2 (%)	Scenario1	Scenario2
	R^2		MSE		RMSE		MAPE	
Random Forest Regressor	91.50	81.35	1571	1.04	39	10.19	43	37
XGBoost Regressor	93.99	82.40	1307	0.98	36	9.89	29	40
ExtraTrees Regressor	88.51	77.96	1997	1.20	45	10.94	88	53

With the ML model represented in this study, engineers can accurately estimate the TMs of any three- or four-legged intersection by using only traffic counts from the designated peak hour, the lane configuration of the desired approach, and the type of intersection.

Guidance to Practitioners

In this study, a model to estimate TMs for three- and four-legged intersections was developed. The model was coded in the Python programming language. With this model, it was possible to estimate the TMs of any desired approach using three pieces of information. First was the traffic volume of all approaches at that intersection; second was the type of intersection; and last was the approach lane configuration data. The model developed in this study took these data from each approach as input and provided the user with an estimated TM for the desired approach.

Discussion

In this study, the authors introduced an ML model to predict TMs at signalized intersections. This model was based on TM data from 1242 traffic manual counts conducted at intersections in Ada County, Idaho. Multi-output regression ML models were applied to provide a reliable estimate of TMs at signalized intersections using a combination of numeric and descriptive variables, including approach volumes, intersection type, and lane configuration data. Three ML-based regression models, including Random Forest Regressor, XGBoost Regressor, and ExtraTrees Regressor, were trained to investigate the relationship between approach volumes and the corresponding turning movements. In order to assess the performance of the model, a number of evaluation metrics were computed, including the R^2, MSE, RMSE, and MAPE. The outcomes of the tests demonstrated that the XGBoost Regressor predicted turning movements more accurately with an R^2 of 93.99%. These results demonstrated that the examined methods yielded a dependable and efficient model for estimating TMs. Considering that currently the most common method for obtaining TMs is still manual counting, the suggested approach can be functional in situations where conducting a manual count is impracticable, due to cost or manpower issues. Additionally, it is advantageous for planning new intersections when no historical data are available.

The value of this research is highlighted either when compared to the earlier studies in this area or methods used in practice. This is the first study that attempted to find a relationship between TMs and approach volumes that involved some descriptive features of intersection in the ML model to improve the predictive power of the model by capturing different aspects of it. Besides, most of the current methods for predicting TMs are based on assumed initial

TMs, which undergo an iterative process of fine-tuning and equilibrium, or a comprehensive procedure for modeling transportation planning data. The findings of this study offer traffic engineers and transportation planners a simple and user-friendly methodology for estimating TMs based on approach volumes, lane configuration, and intersection type.

It should be noted that, due to data constraints, the authors only considered peak-hour volumes. However, peak-hour volumes are frequently utilized for operational analysis, optimization, and design at signalized intersections as well as for conducting other transportation research, such as traffic impact studies. Future work can involve broadening the scope of this research to cover other times of day besides peak hours. Another recommendation is to evaluate the model using the data obtained from a new source of manual data. In theory, this method can be used both in real-time and offline. By taking approach volumes and providing turning movements, it could offer real-time turning movements if real-time traffic volumes are available. However, applying this method in the real world and integrating it with traffic signal controllers requires further investigation, which could be an extension of this study. Yet another way of extending this study is to develop models for non-signalized intersections and roundabouts.

References

Alpaydin, E.. (2020). *Introduction to Machine Learning* (Francis Bach, Ed.; 4th ed., Vol. 4). The MIT Press.

Bélisle, F., Saunier, N., Bilodeau, G. A., & Le Digabel, S. (2017). Optimized video tracking for automated vehicle turning movement counts. *Transportation Research Record*, *2645*(1), 104-112. https://doi.org/10.3141/2645-12

Forster, M., & Sober, E. (2011). AIC Scores as Evidence: A Bayesian Interpretation. *Philosophy of Statistics: Volume 7 in Handbook of the Philosophy of Science*, *7*, 535-549. https://doi.org/10.1016/B978-0-444-51862-0.50016-2

Geurts, P., Ernst, D., & Wehenkel, L. (2006). Extremely randomized trees. *Machine Learning*, *63*(1), 3-42. https://doi.org/10.1007/s10994-006-6226-1

Ghanim, M. S., & Shaaban, K. (2019). Estimating turning movements at signalized intersections using artificial neural networks. *IEEE Transactions on Intelligent Transportation Systems*, *20*(5), 1828-1836. https://doi.org/10.1109/TITS.2018.2842147

Ghods, A. H., & Fu, L. (2014). Real-time estimation of turning movement counts at signalized intersections using signal phase information. *Transportation Research Part C: Emerging Technologies*, *47*(P2), 128-138. https://doi.org/10.1016/j.trc.2014.06.010

Han, J., Kamber, M., & Pei, J. (n.d.). Data Mining Concepts and Techniques. In *Elsevier Morgan Kaufmann* (Vol. 1).

Hauer, E., Pagitsas, E., & Shin, B. T. (1981). Estimation of turning flows from automatic counts. *Transportation Research Record*, *795*, 1-7.

Jordan, M., Kleinberg, J., & Schölkopf, B. (2006). *Pattern Recognition and Machine Learning*. Springer Science+ Business Media.

Karapetrovic, J., & Martin, P. T. (2021). Estimation of intersection turning movement flows with the TMERT3 model version: Sensitivity to a widespread detector failure. *International Journal for Traffic and Transport Engineering*, *11*(3), 442-453. https://doi.org/10.7708/ijtte2021.11(3).07

Maher, M. J. (1984). Estimating the turning flows at a junction: A comparison of three models. *Transportation Research Board*, *25*(1), 19-22.

Mahmoud, N., Abdel-Aty, M., Cai, Q., & Yuan, J. (2021). Predicting cycle-level traffic movements at signalized intersections using machine learning models. *Transportation Research Part C: Emerging Technologies*, *124*. https://doi.org/10.1016/j.trc.2020.102930

Mueller, A., & Guido, S. (2016). *Introduction to Machine Learning with Python: A Guide for Data Scientists* (Vol. 1). O'Reilly Media.

Nazari Enjedani, S., & Khanal, M. (2023). Development of a Turning Movement Estimator Using CV Data. *Future Transportation*, *3*(1), 349-367. https://doi.org/10.3390/futuretransp3010021

Nihan, N. L., & Davis, G. A. (1989). Application of prediction-error minimization and maximum likelihood to estimate intersection O-D matrices from traffic counts. *Transportation Science*, *23*(2), 77-90. https://about.jstor.org/terms

Noyce, D. A., Bill, A. R., Chitturi, M. V, & Santiago-Chaparro, K. R. (2019). *Turning Movement Counts on Shared Lanes: Prototype Development and Analysis Procedures Final Report for NCHRP IDEA Project 198*. www.trb.org/idea

Noyce, D., Chittori, M., Santiago-Chaparro, K., & Bill, A. R. (n.d.). *Automated Turning Movement Counts for Shared Lanes Using Existing Vehicle Detection Infrastructure Final Report for NCHRP IDEA Project 177*.

Pratelli, A., Sordi, L., & Farina, A. (2021). Methods to generate an expected turning traffic flows matrix for road junction analysis. *International Journal of Transport Development and Integration*, *5*(1), 1-14. https://doi.org/10.2495/TDI-V5-N1-1-14

Project Traffic Forecasting Handbook. (2014). Florida Department Transportation.

Saldivar-Carranza, E. D. (2021). *Scalable Operational Traffic Signal Performance Measures from Vehicle Trajectory Data* (Thesis). Purdue University.

Saldivar-Carranza, E. D., Li, H., & Bullock, D. M. (2021). Identifying Vehicle Turning Movements at Intersections from Trajectory Data. *IEEE Conference on Intelligent Transportation Systems, Proceedings, ITSC*, *2021-September*, 4043-4050. https://doi.org/10.1109/ITSC48978.2021.9564781

Santhanam, R., Uzir, N., Raman, S., & Banerjee, S. (2016). Experimenting XGBoost Algorithm for Prediction and Classification of Different Datasets. *International Journal of Control Theory and Applications*, *9*. https://www.researchgate.net/publication/318132203

Santiago-Chaparro, K. R., Chitturi, M., Bill, A., & Noyce, D. A. (2016). Automated turning movement counts for shared lanes: Leveraging vehicle detection data. *Transportation Research Record*, *2558*, 30-40. https://doi.org/10.3141/2558-04

Segal, M. (2003). Machine Learning Benchmarks and Random Forest Regression. Technical Report, Center for Bioinformatics & Molecular Biostatistics, University of California, San Francisco. https://www.researchgate.net/publication/228861739_Machine_Learning_Benchmarks_and_Random_Forest_Regression

Shaaban, K., Hamdi, A., Ghanim, M., & Shaban, K. B. (2022). Machine learning-based multi-target regression to effectively predict turning movements at signalized intersections. *International Journal of Transportation Science and Technology*. https://doi.org/10.1016/j.ijtst.2022.02.003

Shirazi, M. S., & Morris, B. (2014). Vision-Based Turning Movement Counting at Intersections by Cooperating Zone and Trajectory Comparison Modules. *2014 17th IEEE International Conference on Intelligent Transportation Systems, ITSC 2014*, 3100-3105. https://doi.org/10.1109/ITSC.2014.6958188

Shirazi, M. S., & Morris, B. T. (2016). Vision-based turning movement monitoring: Count, speed & waiting time estimation. *IEEE Intelligent Transportation Systems Magazine*, *8*(1), 23-34. https://doi.org/10.1109/MITS.2015.2477474

Vanderplas, J. T. (2016). *Python data science handbook : essential tools for working with data*. O'Reilly Media, Inc.

Vigos, G., & Papageorgiou, M. (2010). A simplified estimation scheme for the number of vehicles in signalized links. *IEEE Transactions on Intelligent Transportation Systems*, *11*(2), 312-321. https://doi.org/10.1109/TITS.2010.2042807

Virkler, M. R., & Kumar, N. R. (1998). System to identify turning movements at signalized intersections. *Journal of Transportation Engineering*, *124*(6).

Yi, P., & Zhang, S. (2017). *Development and Field Testing of an Automatic Turning Movement Identification System*. (Ohio Department of Transportation, State Job Number 135141). https://rosap.ntl.bts.gov/view/dot/36334

Zheng, J., & Liu, H. X. (2017). Estimating traffic volumes for signalized intersections using connected vehicle data. *Transportation Research Part C: Emerging Technologies*, *79*, 347-362. https://doi.org/10.1016/j.trc.2017.03.007

Biographies

SOMAYEH NAZARI ENJEDANI is a graduate student at Boise State University. Nazari Enjedani may be reached at somayehnazarienjedani@u.boisestate.edu

MANDAR KHANAL is a full professor in the Civil Department at Boise State University. Dr. Khanal may be reached at mkhanal@boisestate.edu

Augmented Reality in Foot Palpation: Enhancing Accuracy and Training Medial Cuneiform Bone Localization

Michael U. Dakeev, Sam Houston State University; Suleiman Obeidat, Sam Houston State University; Fatih Demiroz, Sam Houston State University; Vicente Lombardo, Sam Houston State University

Abstract

Palpation, a fundamental technique in medical examination, relies heavily on the practitioner's tactile skills and anatomical knowledge. In this paper, the authors present an innovative approach for enhancing palpation training and practice using augmented reality (AR) technology, specifically focusing on foot examination. The development of expertise in palpation techniques typically requires extensive practice and patient interaction, which can be time-consuming and may not always provide consistent learning experiences for students. To address these challenges, the authors developed an augmented reality application designed to assist in foot palpation training. The aim of the proposed AR application was to provide real-time guidance by visually overlaying palpation zones on a scanned image of the patient's foot, thereby supporting the learning process for new professionals and students.

In this study, the authors compared the accuracy of locating the medial cuneiform bone using traditional methods versus the proposed AR app. Results from a paired-samples t-test ($n = 30$) demonstrated a statistically significant improvement in accuracy when using the AR app ($M = 4.55$ cm, $SD = 0.53$) compared to traditional methods ($M = 9.28$ cm, $SD = 3.24$, $p < 0.001$). The mean improvement of 4.73 cm (95% CI: 3.52 to 5.94) highlights the potential of AR technology for enhancing anatomical education and improving clinical skills. These findings suggest that AR-assisted palpation training could significantly enhance the learning experience, potentially leading to improved diagnostic accuracy and procedural outcomes in clinical settings.

Introduction

The acquisition of proficient palpation skills is a critical component of medical education, particularly in areas such as podiatry and osteopathic. However, traditional teaching methods often struggle to bridge the gap between theoretical knowledge and practical application, especially when dealing with complex anatomical regions like the foot. Palpation is a critical skill in medical diagnosis and treatment, requiring direct physical contact between the healthcare professional and the patient (Canton et al., 2024). The accuracy and effectiveness of palpation depends largely on the practitioner's ability to locate and interpret anatomical structures through touch. However, developing this expertise is a time-consuming process that demands extensive practice and patient interaction. The challenges associated with acquiring proficiency in palpation techniques have long been recognized in medical education. Traditional teaching methods often struggle to bridge the gap between theoretical knowledge and practical application, particularly in complex anatomical regions such as the foot (Muangpoon, Haghighi Osgouei, Escobar-Castillejos, Kontovounisios & Bello, 2020). This gap can lead to inconsistencies in diagnosis and treatment, especially among novice practitioners and students. To address these challenges, this research team developed an augmented reality application designed to assist in foot palpation. This technology aimed to provide real-time guidance by visually overlaying palpation zones on a scanned image of the patient's foot, thereby supporting the learning process for new professionals and students. By integrating AR into palpation training, the authors sought to accelerate the development of muscle memory and improve the accuracy of anatomical localization.

Literature

The importance of palpation in medical practice has been well-documented across various specialties. Studies have shown that accurate palpation skills are crucial for diagnosing musculoskeletal disorders, identifying vascular issues, and assessing soft-tissue abnormalities. However, research also highlights the significant variability in palpation accuracy among practitioners, emphasizing the need for improved training methods. Recent advancements in medical education have seen an increased interest in technology-enhanced learning. Virtual reality (VR) and augmented reality (AR) have emerged as promising tools for medical training, offering immersive and interactive experiences that complement traditional teaching methods (Solutions, 2023; Tene, Vique López, Valverde Aguirre, Orna Puente & Vacacela Gomez, 2024).

Several studies have explored the use of AR in anatomy education, demonstrating improved spatial understanding and knowledge retention among students (Dhar, Rocks, Samarasinghe, Stephenson & Smith, n.d.; Suarez-Rivas, n.d.). In the context of palpation training, haptic feedback systems have been developed to simulate tissue properties and provide a more realistic learning experience. However, these systems often lack the ability to adapt to individual patient anatomies and real-world variations (Sharma, Doherty & Dong, 2017). AR technology offers a unique

solution by overlaying digital information onto the physical world, allowing for personalized guidance in real-time (Dakeev, Pecen, Yildiz & Luong, 2021; MGH Institute, 2024). While AR applications have been successfully implemented in various medical procedures, such as surgery and needle placement, their potential in palpation training remains largely unexplored (MGH Institute, 2024; Tokuç & Varol, 2023). This gap in the literature presents an opportunity to investigate the effectiveness of AR in enhancing palpation skills, particularly in complex anatomical regions like the foot (Condino et al., 2016).

Methodology

In this study, the authors employed a mixed-methods approach to develop and evaluate an AR application for foot palpation training. The methodology consisted of three main phases: application development, user testing, and performance evaluation. The AR application was developed using Unity Game Engine, which allows for real-time scanning and overlaying the patient's foot (Dakeev & Yildiz, 2022). Figure 1 shows how the application incorporates an overlaid image of foot structures, including bones, muscles, ligaments, and key palpation points.

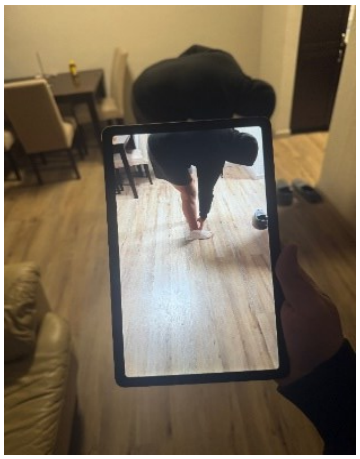

Figure 1. Overlaid image of a foot with bone structures on a Tablet camera.

A sample of 30 participants, including medical students, physiotherapy students, and novice practitioners, as well as randomly selected students (regardless of their background) were recruited for the user testing phase. Researchers asked the participants to locate medial cuneiform bone on the foot. Figure 2 shows how, after marking the pointed zone, the AR application was used to show the correct zone. The researchers measured the distance between the marked location that the participant showed and the AR application's located zone. Data collection methods included pre- and post-training assessments of palpation accuracy, surveys to evaluate user experience and perceived effectiveness, and observational analysis of the palpation technique. Participants were assessed on their ability to accurately locate medial cuneiform, apply appropriate pressure during palpation, and feel the applied pressure. Using SPSS statistical analysis package, the researchers conducted a paired-sample t-test to compare the performance of the control and experimental groups. This methodology aimed to provide a comprehensive evaluation of the AR application's effectiveness in enhancing foot palpation skills among novice practitioners and students.

The participants were asked to indicate the palpation zone on their feet using their fingers after which the AR system identified and recorded the corresponding location. The measured difference between the participant-indicated zone and the AR-identified zone served as the primary metric. However, due to individual physiological variations, no standardized mean value exists for the palpation zone. In clinical practice, physicians typically rely on experience and anatomical knowledge to estimate this location, as it varies from patient to patient. Consequently, a traditional measurement mean could not be established in this study. The authors further sought to gain insights into both the practical benefits and the user experience of integrating AR technology into palpation training.

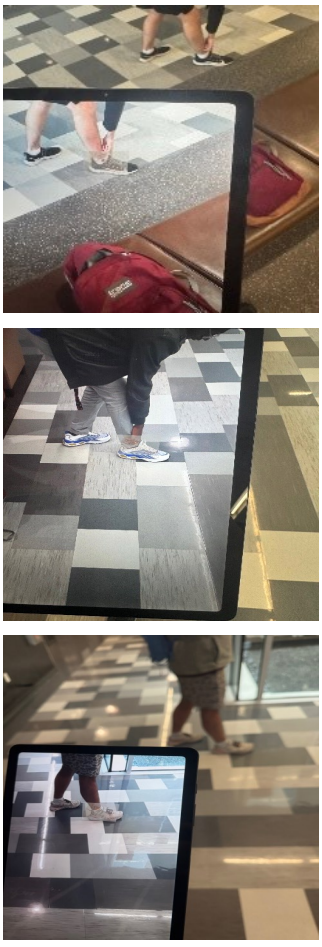

Figure 2. Locating palpation zone with the AR application.

Data Analysis

A paired-samples t-test was conducted to compare the accuracy of locating the medial cuneiform bone using traditional methods and an AR app. Tables 1 and 2 provide the descriptive statistics for the paired-sample correlations, which revealed that there was a weak negative correlation between the traditional method (M = 9.28, SD = 3.24) and the AR app method (M = 4.55, SD = 0.53), r = −0.047, p = 0.805 (two-tailed). This correlation was not statistically significant, indicating that performance on one method did not reliably predict performance on the other.

Table 1. Paired-sample descriptive statistics to locate the palpation zone.

		Mean	N	Std. deviation	Std. error mean
Pair 1	Traditional	9.266	30	3.172	0.579
	AR_APP	4.533	30	0.524	0.095

Table 2. Paired-sample correlations between traditional location versus AR application.

				Significance	
		N	Correlation	One-sided *p*	Two-sided *p*
Pair 1	Traditional & AR_APP	30	-0.047	0.403	0.805

Table 3 shows the paired-samples t-test, which revealed a statistically significant difference between the traditional palpation method and the AR-assisted method, t(29) = 8.003, p < 0.001 (two-tailed). The mean deviation was 4.73 cm (95% CI: 3.52 to 5.94), with the traditional method showing greater inaccuracy (M = 9.28 cm) compared to the AR-guided approach (M = 4.55 cm). These values represent the average deviation across all participants, not individual measurements. The marked reduction in deviation from 9.3 cm to 4.5 cm suggests that the AR tool significantly improved the accuracy of locating the palpation zone. Given the absence of a standardized anatomical landmark for this procedure, healthcare professionals typically rely on their clinical experience and subjective judgment to identify the correct location. As a result, there is inherent variability in technique and accuracy across practitioners. In this study, the authors aimed to provide a more standardized reference for novice learners by using AR technology to reduce reliance on years of experience and to guide students toward more accurate palpation with reduced error margins.

These outcomes provide strong evidence for the effectiveness of the AR app in improving the accuracy of locating the medial cuneiform bone compared to traditional methods. The significant decrease in mean distance from 9.28 cm (traditional method) to 4.55 cm (AR app method) represents a substantial improvement in precision. The lack of significant correlation between the two methods suggests that the participants' performance with the traditional method did not predict their performance with the AR app. This independence between the two approaches highlights the potential of the AR app to provide consistent benefits across various skill levels. The large t-statistic (8.003) and the small p-value (< 0.001) indicate that the observed difference between the two methods is highly unlikely to have occurred by chance. The 95% confidence interval of the difference (3.52 to 5.94 cm) does not include zero, further supporting the conclusion that the AR app method consistently outperformed the traditional method. These findings have important implications for medical education and clinical practice. The AR app demonstrated an advantage in improving the accuracy of anatomical localization, which could lead to enhanced diagnostic and procedural skills. Future research should explore the long-term retention of these skills and the transferability of AR-assisted learning to other anatomical structures and medical procedures.

Conclusions

In this study, the authors investigated the effectiveness of an augmented reality app compared to traditional methods in accurately locating the medial cuneiform bone. A paired-samples t-test showed that the AR application (M = 4.55 cm, SD = 0.53) demonstrated significantly higher accuracy in locating the medial cuneiform bone for palpation compared to the traditional method (M = 9.28 cm, SD = 3.24) for randomly selected untrained students with different backgrounds. There was a statistically significant difference between the two methods (p < 0.001), with a mean improvement of 4.73 cm (95% CI: 3.52 to 5.94) when

Table 3. Paired-sample t-test.

					95% Confidence interval of the difference				Significance	
		Mean	Std. deviation	Std. error mean	Lower	Upper	t	df	One-sided *p*	Two-sided *p*
Pair 1	Traditional AR_APP	4.73333	3.23966	0.59148	3.52362	5.94304	8.003	29	< 0.001	< 0.001

using the AR app. Furthermore, the correlation between performances on the two methods was weak and non-significant ($r = -0.047$, $p = 0.805$), suggesting that the AR app's benefits were consistent across participants regardless of their performance with the traditional method. The researchers believe this study provides compelling evidence for the superiority of the AR app over traditional methods in improving the accuracy of locating the medial cuneiform bone. The significant reduction in localization error demonstrated the potential of AR technology to enhance anatomical education and clinical skills.

These findings have important implications for medical training, potentially leading to improved diagnostic accuracy and procedural outcomes in clinical settings. Future research should focus on the long-term retention of skills acquired through AR-assisted learning, its applicability to other anatomical structures, and its integration into broader medical education curricula. Additionally, investigating the impact of AR-enhanced anatomical learning on clinical performance and patient outcomes would further establish the value of this technology in healthcare education and practice.

References

Canton, S. P., Austin, C. N., Steuer, F., Dadi, S., Sharma, N., Kass, N. M. ...Hogan, M. V. (2024). Feasibility and Usability of Augmented Reality Technology in the Orthopaedic Operating Room. *Current Reviews in Musculoskeletal Medicine*, *17*(5), 117-128. https://doi.org/10.1007/s12178-024-09888-w

Condino, S., Viglialoro, R., Fani, S., Bianchi, M., Morelli, L., Ferrari, M. …Ferrari, V. (2016). *Tactile Augmented Reality for Arteries Palpation in Open Surgery Training* (p. 197). https://doi.org/10.1007/978-3-319-43775-0_17

Dakeev, U., Pecen, R., Yildiz, F., & Luong, Y. (2021). Augmented Reality Computer-aided Design Education (ARCADE) Tool to Improve Student Motivation, Engagement, and Spatial Cognition. *2021 ASEE Virtual Annual Conference Content Access Proceedings*, 36730. https://doi.org/10.18260/1-2--36730

Dakeev, U., & Yildiz, F. (2022). *Design and Development of Mixed Reality (MR) Laboratory Tools to Improve Spatial Cognition, Student Engagement, and Employee Safety*. https://doi.org/10.5281/ZENODO.7332034

Dhar, P., Rocks, T., Samarasinghe, R. M., Stephenson, G., & Smith, C. (n.d.). Augmented reality in medical education: Students' experiences and learning outcomes. *Medical Education Online*, *26*(1), 1953953. https://doi.org/10.1080/10872981.2021.1953953

MGH Institute. (2024, May 17). Integrating Technology in Health Professions Education: Trends and Innovations. MGH IHP. https://www.mghihp.edu/news-and-more/opinions/health-professions-education-effects/integrating-technology-health-professions-education-trends-and-innovations

Muangpoon, T., Haghighi Osgouei, R., Escobar-Castillejos, D., Kontovounisios, C., & Bello, F. (2020). Augmented Reality System for Digital Rectal Examination Training and Assessment: System Validation. *Journal of Medical Internet Research*, *22*(8), e18637. https://doi.org/10.2196/18637

Sharma, N., Doherty, I., & Dong, C. (2017). Adaptive Learning in Medical Education: The Final Piece of Technology Enhanced Learning? *The Ulster Medical Journal*, *86*(3), 198-200.

Solutions, H. (2023, November 14). *Augmented Reality (AR) in Medical Training: The Next Frontier in Healthcare Education*. Holon Solutions. https://www.holonsolutions.com/augmented-reality-ar-in-medical-training-the-next-frontier-in-healthcare-education/

Suarez-Rivas, M. (n.d.). *Can Augmented Reality Improve the Learning Experience of Future Healthcare Professionals? (2022)*. https://www.visiblebody.com/blog/can-augmented-reality-increase-anatomy-learning-for-future-healthcare-professionals

Tene, T., Vique López, D. F., Valverde Aguirre, P. E., Orna Puente, L. M., & Vacacela Gomez, C. (2024). Virtual reality and augmented reality in medical education: An umbrella review. *Frontiers in Digital Health*, *6*. https://doi.org/10.3389/fdgth.2024.1365345

Tokuç, B., & Varol, G. (2023). Medical Education in the Era of Advancing Technology. *Balkan Medical Journal*, *40*(6), 395-399. https://doi.org/10.4274/balkanmedj.galenos.2023.2023-7-79

Biographies

MICHAEL U. DAKEEV is an associate professor and program coordinator of Engineering Design Technology at Sam Houston State University. He holds a PhD in Technology, an MS in Industrial Management, and a BS in Industrial Engineering. Dr. Dakeev's work focuses on applied engineering education, certification training, and immersive learning through AR/VR tools. Dr. Dakeev may be reached at dakeev@shsu.edu

SULEIMAN OBEIDAT is an assistant professor at Sam Houston State University. He received his PhD in Industrial Engineering from the University of Oklahoma. Dr. Obeidat's research focuses on additive manufacturing and inspection of machined surfaces using coordinate machines (CMM). Dr. Obeidat may be reached at obeidat@shsu.edu

FATIH DEMIROZ is an associate professor at SHSU. He received his PhD in Public Affairs from the University of Central Florida. His research interests focus on complex socio-technical systems, networks, and disaster management. Dr. Demiroz may be reached at fxd009@shsu.edu

VICENTE LOMBARDO is a senior in the Engineering Design Technology program at Sam Houston State University. He has a strong interest in mechanical design, manufacturing processes, and hands-on engineering applications. Throughout his time at SHSU, Vicente has worked on multiple team-based design projects and continues to develop his skills in CAD modeling, 3D printing, and CNC machining. He aims to pursue a career in advanced manufacturing or product development after graduation. Vicente may be reached at vjl009@shsu.edu

INSTRUCTIONS FOR AUTHORS: MANUSCRIPT FORMATTING REQUIREMENTS

The INTERNATIONAL JOURNAL OF MODERN ENGINEERING is an online/print publication designed for Engineering, Engineering Technology, and Industrial Technology professionals. All submissions to this journal, submission of manuscripts, peer-reviews of submitted documents, requested editing changes, notification of acceptance or rejection, and final publication of accepted manuscripts will be handled electronically. The only exception is the submission of separate high-quality image files that are too large to send electronically.

All manuscript submissions must be prepared in Microsoft Word (.doc or .docx) and contain all figures, images and/or pictures embedded where you want them and appropriately captioned. Also included here is a summary of the formatting instructions. You should, however, review the sample Word document on our website (http://ijme.us/formatting_guidelines/) for details on how to correctly format your manuscript. The editorial staff reserves the right to edit and reformat any submitted document in order to meet publication standards of the journal.

The references included in the References section of your manuscript must follow APA-formatting guidelines. In order to help you, the sample Word document also includes numerous examples of how to format a variety of scenarios. Keep in mind that an incorrectly formatted manuscript will be returned to you, a delay that may cause it (if accepted) to be moved to a subsequent issue of the journal.

1. **Word Document Page Setup:** Two columns with ¼" spacing between columns; top of page = ¾"; bottom of page = 1" (from the top of the footer to bottom of page); left margin = ¾"; right margin = ¾".

2. **Paper Title:** Centered at the top of the first page with a 22-point Times New Roman (Bold), small-caps font.

3. **Page Breaks:** Do not use page breaks.

4. **Figures, Tables, and Equations:** All figures, tables, and equations must be placed immediately after the first paragraph in which they are introduced. And, each must be introduced. For example: "Figure 1 shows the operation of supercapacitors." "The speed of light can be determined using Equation 4:"

5. **More on Tables and Figures:** Center table captions above each table; center figure captions below each figure. Use 9-point Times New Roman (TNR) font. Italicize the words for table and figure, as well as their respective numbers; the remaining information in the caption is not italicized and followed by a period—e.g., "*Table 1*. Number of research universities in the state." or "*Figure 5*. Cross-sectional aerial map of the forested area."

6. **Figures with Multiple Images:** If any given figure includes multiple images, do NOT group them; they must be placed individually and have individual minor captions using, "(a)" "(b)" etc. Again, use 9-point TNR.

7. **Equations:** Each equation must be numbered, placed in numerical order within the document, and introduced—as noted in item #4.

8. **Tables, Graphs, and Flowcharts:** All tables, graphs, and flowcharts must be created directly in Word; tables must be enclosed on all sides. The use of color and/or highlighting is acceptable and encouraged, if it provides clarity for the reader.

9. **Textboxes:** Do not use text boxes anywhere in the document. For example, table/figure captions must be regular text and not attached in any way to their tables or images.

10. **Body Fonts:** Use 10-point TNR for body text throughout (1/8" paragraph indention); indent all new paragraphs as per the images shown below; do not use tabs anywhere in the document; 9-point TNR for author names/affiliations under the paper title; 16-point TNR for major section titles; 14-point TNR for minor section titles.

11. **Personal Pronouns:** Do not use personal pronouns (e.g., "we" "our" etc.).

12. **Section Numbering:** Do not use section numbering of any kind.

13. **Headers and Footers:** Do not use either.

14. **References in the Abstract:** Do NOT include any references in the Abstract.

15. **In-Text Referencing:** For the first occurrence of a given reference, list all authors—last names only—up to seven (7); if more than seven, use "et al." after the seventh author. For a second citation of the same reference—assuming that it has three or more authors—add "et al." after the third author. Again, see the *sample Word document* and the *formatting guide for references* for specifics.

16. **More on In-Text References:** If you include a reference on any table, figure, or equation that was not created or originally published by one or more authors on your manuscript, you may not republish it without the expressed, written consent of the publishing author(s). The same holds true for name-brand products.

17. **End-of-Document References Section:** List all references in alphabetical order using the last name of the first author—last name first, followed by a comma and the author's initials. Do not use retrieval dates for websites.

18. **Author Biographies:** Include biographies and current email addresses for each author at the end of the document.

19. **Page Limit:** Manuscripts should not be more than 15 pages (single-spaced, 2-column format, 10-point TNR font).

20. **Page Numbering:** Do not use page numbers.

21. **Publication Charges:** Manuscripts accepted for publication are subject to mandatory publication charges.

22. **Copyright Agreement:** A copyright transfer agreement form must be signed by all authors on a given manuscript and submitted by the corresponding author before that manuscript will be published. Two versions of the form will be sent with your manuscript's acceptance email.

    Only one form is required. Do not submit both forms!

    The form named "paper" must be hand-signed by each author. The other form, "electronic," does not require hand signatures and may be filled out by the corresponding author, as long as he/she receives written permission from all authors to have him/her sign on their behalf.

23. **Submissions:** All manuscripts and required files and forms must be submitted electronically to Dr. Philip D. Weinsier, manuscript editor, at philipw@bgsu.edu.

24. **Published Deadlines:** Manuscripts may be submitted at any time during the year, irrespective of published deadlines, and the editor will automatically have your manuscript reviewed for the next-available issue of the journal. Published deadlines are intended as "target" dates for submitting new manuscripts as well as revised documents. Assuming that all other submission conditions have been met, and that there is space available in the associated issue, your manuscript will be published in that issue if the submission process—including payment of publication fees—has been completed by the posted deadline for that issue.

    Missing a deadline generally only means that your manuscript may be held for a subsequent issue of the journal. However, conditions exist under which a given manuscript may be rejected. Always check with the editor to be sure. Also, if you do not complete the submission process (including all required revisions) within 12 months of the original submission of your manuscript, your manuscript may be rejected or it may have to begin the entire review process anew.

CUTTING EDGE JOURNAL OF RESEARCH AND INNOVATION IN ENGINEERING

Print ISSN: 2152-4157
Online ISSN: 2152-4165

www.ijeri.org

www.iajc.org

INTERNATIONAL JOURNAL OF ENGINEERING RESEARCH AND INNOVATION

ABOUT IJERI:

- IJERI is the second official journal of the International Association of Journals and Conferences (IAJC).
- IJERI is a high-quality, independent journal steered by a distinguished board of directors and supported by an international review board representing many well-known universities, colleges, and corporations in the U.S. and abroad.
- IJERI has an impact factor of **1.58**, placing it among an elite group of most-cited engineering journals worldwide.

OTHER IAJC JOURNALS:

- The International Journal of Modern Engineering (IJME) For more information visit www.ijme.us
- The Technology Interface International Journal (TIIJ) For more information visit www.tiij.org

IJERI SUBMISSIONS:

- Manuscripts should be sent electronically to the manuscript editor, Dr. Philip Weinsier, at philipw@bgsu.edu.

  For submission guidelines visit www.ijeri.org/submissions

TO JOIN THE REVIEW BOARD:

- Contact the chair of the International Review Board, Dr. Philip Weinsier, at philipw@bgsu.edu.

  For more information visit www.ijeri.org/editorial

INDEXING ORGANIZATIONS:

- IJERI is currently indexed by 16 agencies. For a complete listing, please visit us at www.ijeri.org.

Contact us:

Mark Rajai, Ph.D.

Editor-in-Chief
California State University-Northridge
College of Engineering and Computer Science
Room: JD 4510
Northridge, CA 91330
Office: (818) 677-5003
Email: mrajai@csun.edu

www.tiij.org

www.ijme.us

THE LEADING JOURNAL OF ENGINEERING, APPLIED SCIENCE AND TECHNOLOGY

The latest impact factor (IF) calculation (Google Scholar method) for IJME of 3.0 moves it even higher in its march towards the top 10 engineering journals.

IJME IS THE OFFICAL AND FLAGSHIP JOURNAL OF THE INTERNATIONAL ASSOCATION OF JOURNALS AND CONFERENCE (IAJC)
www.iajc.org

The International Journal of Modern Engineering (IJME) is a highly-selective, peer-reviewed journal covering topics that appeal to a broad readership of various branches of engineering and related technologies. IJME is steered by the IAJC distinguished board of directors and is supported by an international review board consisting of prominent individuals representing many well-known universities, colleges, and corporations in the United States and abroad.

IJME Contact Information

General questions or inquiries about sponsorship of the journal should be directed to:

Mark Rajai, Ph.D.
Editor-in-Chief
Office: (818) 677-5003
Email: editor@ijme.us
Department of Manufacturing Systems Engineering & Management
California State University-Northridge
18111 Nordhoff St.
Northridge, CA 91330